Title
Gigahertz Non-Volatile Voltage Tuned Magnetic Film Inductors using a Ni/NiFe Core

Author
Lewis, Mark Dylan

Publication Date
2012

Peer reviewed|Thesis/dissertation

UNIVERSITY OF CALIFORNIA

Los Angeles

Gigahertz Non-Volatile Voltage Tuned Magnetic Film Inductors using a Ni/NiFe Core

A thesis submitted in partial satisfaction

of the requirements for the degree Master of Science

in Electrical Engineering

by

Mark Dylan Lewis

2012

ABSTRACT OF THE THESIS

Gigahertz Non-Volatile Voltage Tuned Magnetic

Film Inductors using a Ni/NiFe Core

by

Mark Dylan Lewis

Master of Science in Electrical Engineering

University of California, Los Angeles, 2012

Professor Kang L. Wang, Chair

Magnetic film inductors show promise for increasing the inductance density, and thus shrinking the size, of integrated inductors. With a higher inductance density, integrated inductors can improve RF circuit performance. The ability to individually tune the integrated inductors using an applied voltage has been researched in recent years, often using MEMS type devices. This study utilized the properties of multiferroics to achieve voltage tuned inductance for microstrip inductors. The microstrip inductors demonstrated inductance enhancement up to 75%, a maximum tuning of 25%, and to have operating frequency up to 2.4 GHz, important

for microwave applications. The quality factor of the inductor was enhanced by 170% from the air-core inductor. Taking advantage of the properties of the two-phase multiferroic, the inductance change was also demonstrated to be non-volatile. The unique properties of this inductor allow for both discrete non-volatile, as well as continuous, tuning of the inductance at GHz frequencies.

The thesis of Mark Dylan Lewis.

Robert Candler

Oscar Stafsudd

Kang Wang, Committee Chair

University of California, Los Angeles
2012

Table of Contents

List of Figures

List of Tables

Acknowledgements

First I would like to thank my adviser, Professor Kang L. Wang, for providing me with the opportunity and guidance through my graduate studies. His passion for research and drive for a deeper understanding taught me how to approach a research topic. Without his understanding and encouragement during personal challenges, I would not have been able to finish this project. Thank you Professor Wang for all your support during my graduate studies.

I would also like to thank Dr. Pedram Khalili for all of his help from project conception through final measurements. His patient help and guidance for the understanding of challenges faced during research were invaluable for the completion of the project. Thank you to everyone in the Device Research Lab (DRL) who helped me throughout my graduate studies, from equipment training, to fabrication advice, to a deeper understanding of the physics involved, I learned so much from the other students and postdocs in the lab.

This work would not have been possible without the support from our collaborators with the DARPA STT-RAM and NVL projects, as well as the funding received through the Clean Green IGERT. Fabrication of the final devices would not have been possible without the UCLA Nanolab Cleanroom, CNSI Integrated Systems Nanofabrication Cleanroom (ISNC), and all the staff help received from both.

Lastly I would like to thank my friends and family for all the support during my graduate studies

Introduction

The high demand for decreasing the size and weight of communication devices has been a strong motivation for researching improvements of monolithic inductors. [1,2] The inductor is the least compatible passive device with silicon integration and subsequent scaling, [1] and is often used in RF applications as a discrete device rather than integrated into the Silicon chip. [3] The bulkiness of the discrete inductors has been a disadvantage for use in portable electronic devices, and so inductors that incorporate magnetic films to boost inductance densities have been researched recently. [3] The use of magnetic films shows potential for completely integrated inductors that have significantly higher inductance density and thus take up less space, ideal for portable electronics. [1-3] The size difference for discrete passives and embedded passives is depicted in figure 1 below, with integrated devices having even larger space saving potential by being fabricated directly on the IC chip. [3]

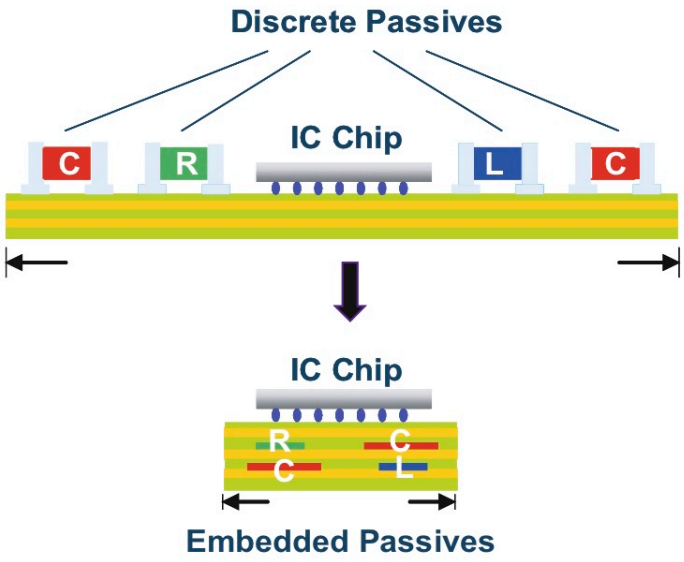

Figure 1: Schematic depiction of the difference between discrete passive devices and embedded passives used in RF circuits. [2]

Another challenge faced by integrated devices is the ability to tune the desired frequency. With discrete inductors, the entire device can be removed and replaced with an inductor of a different value. [3] If the inductors are integrated, this is not a possibility. Tunable passive devices for use in RF circuits have been investigated in recent years in order to add adaptability for RF applications. [4-6] Variable capacitors have already been demonstrated and are currently used for frequency tuning in LC circuits. [4] The capacitance tuning has been limited, however, and greater frequency tuning can be achieved if the inductors in the LC circuit could be tuned as well. [4]

Magnetic Film Inductors

Background

The current technology used for Silicon integration is an air-core spiral inductor, which has poor scaling properties. The inductance of a spiral inductor should theoretically be proportional to the square of the number of turns. [1] However, in practice it is closer to a linear relationship, with the spiral behaving more like an elongated strip inductor instead of a solenoid type. [1-3] To scale an air-gap spiral inductor, the coils will need to be closer together so that the inductor will take up less area. This will increase the parasitic capacitance, effectively limiting the operating frequency due to its self-resonating frequency. [3] Figure 2 below shows a plot of the demonstrated integrated inductance plotted against both the corresponding self-resonating frequency and resistance. [3] With the desire for devices to be integrated on a single chip, smaller, and still have high frequency operation, new device structures are required. [1-3]

Incorporating magnetic thin films in integrated inductors has the potential to significantly increase the inductance density and quality factor. [7-10] Magnetic thin film inductors were first proposed and demonstrated over 40 years ago using a square spiral

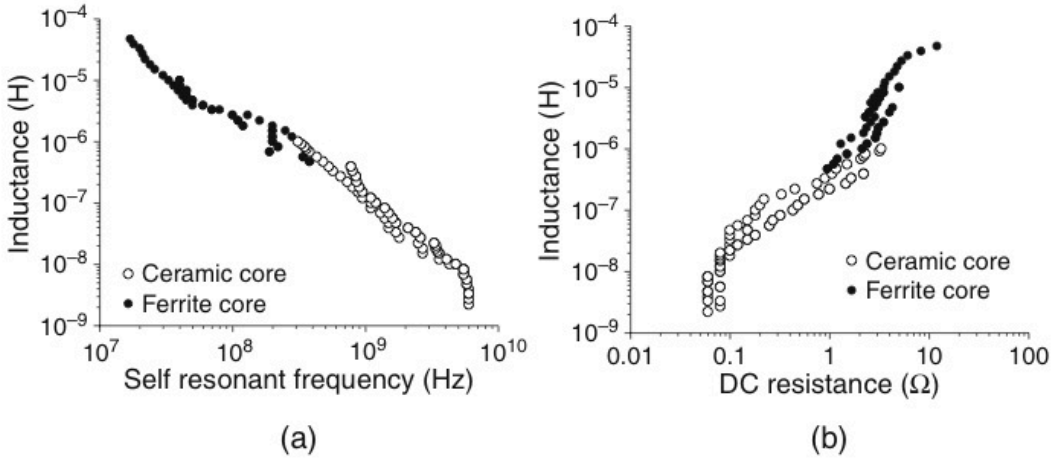

Figure 2: Characteristics of wire-wound inductors currently in use, demonstrating the trade off between high frequency operation and inductance density [3]

inductor with 2 permalloy films, each 0.3μm thick. [7] The inductors showed an enhancement of ~15% with an operating frequency only up to 10MHz. [7] Inductance density and quality factor of magnetic film inductors have been improving ever since. Spiral inductors with the addition of a single magnetic thin film have been demonstrated with gains of 30-60%, [8, 9] closer to the theoretical limit of 100%. [2] Simulations have shown that the addition of 2 layers has the potential for significantly larger increases in inductance density, but experimentally it has been difficult to demonstrate. [2, 8, 9] Simple strip inductors have been easier to demonstrate increased enhancement with two magnetic layers deposited, though these still are far from the theoretical values. [10] Figure 3 summarizes the improvements in inductance density and quality factor using magnetic film inductors for different types of integrated inductor designs. [2] Very few devices have demonstrated both high frequency operation (GHz region) and high inductance density. [2] The challenge with incorporating the magnetic films into integrated inductors is to use enough magnetic material to achieve a large inductance gain, but to keep the material thin enough to reduce losses. [1-3]

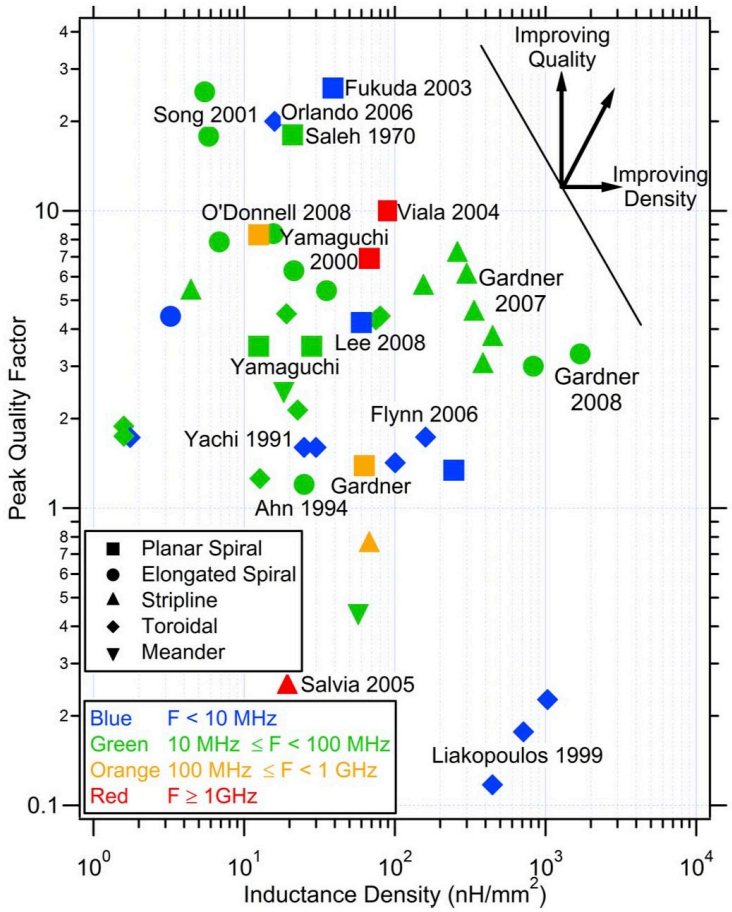

Figure 3: Plot of the inductance density vs. peak quality factor for reported inductors. Color indicates frequency while shape indicates inductor design.[2]

Magnetic Materials

The choice of the magnetic material for use in integrated inductors is important for inductance enhancement as well as frequency response. [1,2] There are three main material properties to use in determining the magnetic film: magnetic saturation (M_s), anisotropy (H_a), and resistivity (ρ). [1] The permeability (μ_r) of the material will determine the inductance enhancement based on how much area the magnetic core (A_{MC}) takes up of the total core area (A_{AC}) (equation 1, inductance gain of a solenoid with magnetic core). [2, 11]

$$\frac{\Delta L}{L_0} = \mu_r \frac{A_{MC}}{A_{AC}} \quad (1)$$

$$\mu_r = \frac{4\pi M_S}{H_{eff}+1} \quad (2)$$

$$H_{eff} = H_a + H_{ext} \quad (3)$$

The permeability is calculated using equation 2, confirming that the material needs a high M_s and a low H_a to have the highest inductance gain. The low anisotropy field is important because it will also ensure minimal hysteresis loss. [3] Balanced against this need for low anisotropy for minimizing loss is the ferromagnetic resonance (FMR) frequency, determined using equation 4, which increases with increasing H_a. [11] The permeability in ferromagnetic films will become mostly imaginary at the FMR frequency, effectively making the inductor into a resistor. [1-3] Therefore the operating frequency will need to be below the FMR frequency, and the magnetic film needs to have a thin FMR line width to maintain high frequency performance. [1] Preferably, a controllable anisotropy is desired so the balance between equation 2 and 4 can be tuned for the desired application.

$$f_{FMR} = \frac{\gamma \mu_0}{2\pi} \sqrt{M_s \cdot H_{eff}} \quad (4)$$

For magnetic thin films, there are two main components to the anisotropy that will determine its magnitude: the internal magnetic anisotropy energy (MAE) and the shape anisotropy. [57] MAE is the energy in the ferromagnetic crystal that will direct the magnetization along a preferred axis. This energy is very small compared to the total energy per atom (0.2μeV/atom for MAE compared to 10μeV/atom total). [57] For thin films and multilayers, the reduced symmetry at the surfaces and the distortion of the lattice due to strain can cause significant increase in the MAE by orders of magnitude. [57] In thin films, the shape anisotropy also becomes important. It arises from the long-range dipolar interactions between the moments, allowing its value to be strongly influenced by shape. [57] The shape can be effectively used to tune the anisotropy to a

desired value that can be strong enough to overcome the MAE preferred direction of the materials. [57] By designing the thin films thickness and shape, the anisotropy of the magnetic core can be controlled to a desired value.

One of the major losses the inductor will experience is through eddy currents, which can be reduced by having magnetic thin films with higher resistivity. [12] The frequency at which the eddy current loss will become significant can be determined using the skin depth of the magnetic core (equation 5). [13] The films being used can be kept thinner than the skin depth at the desired frequency, and this will reduce the loss coming from the magnetic flux traveling through the film. [58] One method of keeping eddy current loss low but the total magnetic material high has been to use multilayers with oxide separation so that each layer is below the skin depth thickness. [58] With this method, there are still significant losses at high frequency from the out of plane flux. [58] In order to address this loss mechanism, research has gone into using granular composite magnetic materials, which show promise for low loss magnetic cores. [58] The lower the losses (both for eddy currents and hysteresis loss, as well as for spin-lattice relaxation and spin-waves) the better the high frequency performance of the inductor and the higher the inductance gain can be. [1]

$$f = \frac{\varrho}{\pi \mu_0 \mu_r t_m^2} \quad (5)$$

For use in embedded or integrated devices, the material will also need to be easily deposited using CMOS compatible fabrication tools. The ideal material for use in magnetic inductors will therefore have a high M_s to maximize both inductance gain and FMR frequency. It will need to have a controllable anisotropy so that the balance between high permeability and high FMR frequency (equations 2 and 4) can be tuned for specific applications. Lastly, it will need to have high resistivity to minimize losses due to

eddy currents and be capable of deposition using CMOS compatible fabrication techniques. There are currently two main categories of magnetic materials being investigated for integration with magnetic film inductors that meet these requirements: magnetic oxides and soft magnetic films. [2, 3]

Integrated Magnetic Oxides

Ferrites and other oxides have been investigated for use in magnetic inductors because of their high resistivity. [1] The magnetic oxides are insulators and so loss is minimized, though the other magnetic properties are sacrifices (M_s is at least a factor of 5 lower than soft magnetic materials). Growth of the magnetic oxides is very important for the magnetic properties of the material and poses challenges for integration. [14] Epitaxial grown garnets have shown some of the best FMR line width properties, but they have many disadvantages including low M_s and difficulty with integration due to the need for lattice matched substrates. [14] Polycrystalline ferrite materials have also been investigated for their ease of deposition, but show large FMR line widths and thus high loss and poor frequency response. [14]

Sputtering and pulsed laser deposition methods have also been investigated for ferrites with the as-deposited films having poor magnetic properties and requiring high temperature annealing, not compatible with CMOS integration. [15-16] Though current methods have yielded poor magnetic properties, the high resistivity (and thus low loss) for the magnetic oxides offer a large advantage if the magnetic properties can be improved. [1] Progress has been made, and inductors fabricated using integrated ferrites have been demonstrated recently with significantly improved characteristics. [14] $Ni_{0.4}Zn_{0.4}Cu_{0.2}Fe_2O_4$ was integrated into an inductor structure and inductance enhancement was demonstrated to be a 160% increase over the air-core values and were operable up to 20 GHz because of the high resistivity. [14]

Soft Magnetic Films

Soft magnetic material can be easily deposited onto substrates using many different methods, including e-beam evaporation and sputtering. Permalloy ($Ni_{80}Fe_{20}$) is a well studied material that is easily deposited and commonly used for magnetic inductors and other applications. [17-18] It has moderate M_s (~1.2T) and resistivity (~40μΩ cm), and has been used to demonstrate 100% inductance gain at an operating frequency of 100's of MHz. [18] More materials are being investigated for integration that show even higher M_s and resistivity, showing potential for greater inductance gain and higher frequency operation. [1-3] With the emergence of these improved alloys, and the fact that they are easily deposited and integrated into CMOS type fabrication, much of the research on magnetic inductors has utilized soft magnetic films. [1-3, 17-21]

Research in combining many of the ferromagnetic materials (Fe, CoFe, FeGa, etc.) with a non-magnetic material (B, N, or O) to create an alloy that improves the important magnetic properties has shown promising results. [19-21] Small additions of B or N have been used to not only decrease FMR line width and increase resistivity, but also show great control over these properties by tuning the amount of B or N incorporated. [19,20] Table 1 summarizes the important properties (μ_r, H_a, ρ) for many different soft magnetic materials that can be used.

Materials	Permeability	Resistivity (μΩ-cm)	Coercivity (Oe)
CoZrTA	600-780	100	<1
CoZrNb	850	120	<1
FeCoN	1200	50	<1
CoFeHfO	140-170	1600	<1
FeAlO	500-700	50-2000	
CoFeSiO	200	2200	<1
CoFeAlO	300	200-300	<1
NiFe	800-1000	40	5
CoFeB	800-1000	100	10 to 20

Table 1: Summary of the important magnetic properties of many potential soft magnetic materials that can be used as in integrated magnetic film inductors

Inductor Design

For designing the integrated inductors, there are many options that offer different benefits and challenges. For all design choices, the magnetic field generated by the inductor should be perpendicular to the easy axis of the magnetic core to obtain the largest enhancement. [1-3, 55] There are three main categories that the majority of inductors being researched fall under: strip, spiral, and solenoid. [1-3]

Strip

The simplest inductor design is the sandwich strip inductor, shown in Figure 4a. [10] Sandwich strip inductors have been shown to significantly improve the inductance density, with the inductance (nH/cm) for devices with no gap estimated by calculating the reactance of the sandwiching films (equation 6). [10]

$$\frac{L}{l}=2\pi\mu_r\left(\frac{t_m}{w}\right) \quad (6)$$

For the inductor, the magnetic films surround the conducting strip, and fabrication only requires 1 or 2 photolithography steps. [10, 22] The inductors can be fabricated using a single mask if no oxide is needed between the magnetic films and the conducting metal; by utilizing the different deposition of magnetic films (sputtered) and the conducting metal (evaporated) the two magnetic films will still be able to be in direct contact with only one mask. [22] If a higher Q is desired, an oxide layer can be deposited below and on-top of the conducting layer, isolating it from the magnetic films. Ensuring there is no gap between the magnetic layers significantly improves the enhancement in the inductance. [10, 22] If there is a gap, significant magnetic flux is lost instead of being entirely contained by the high permeability magnetic material. [10, 22] Figure 4b shows the drop off in inductance gain if there is even a small gap present between the magnetic

layers. [22] Monolithic sandwich strip inductors have been fabricated using Fe-N, a high resistivity soft magnetic film, to demonstrate GHz operation. [22]

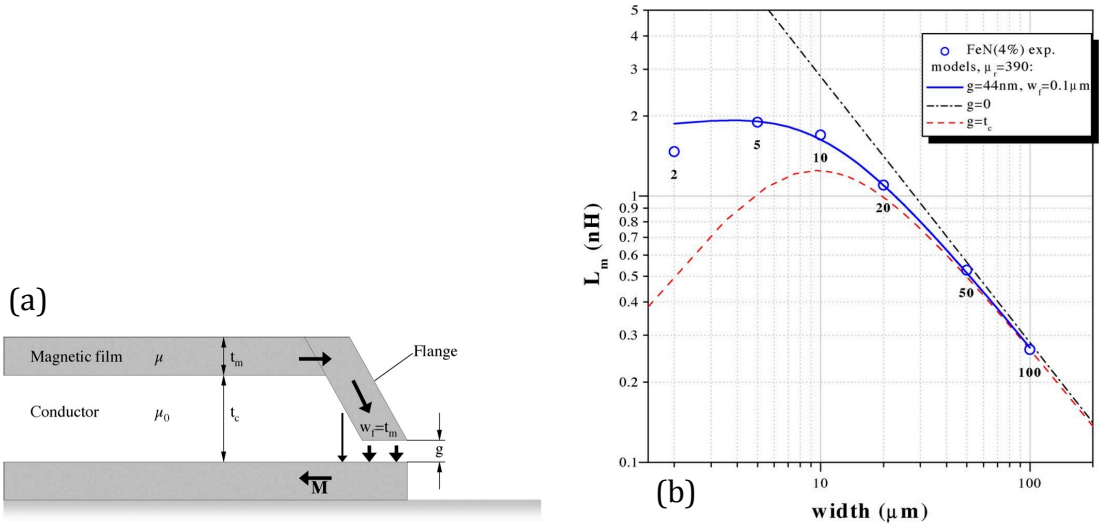

Figure 4: (a) Cross-section of a magnetic sandwich strip inductor, showing the gap between magnetic films with (b) measured and calculated dependence of inductance on the gap width. [22]

Microstrip devices have also been investigated, utilizing magnetic core between the stripline and the ground plane, as shown in figure 5a. A microstrip inductor will have its magnetic field generated between the stripline and ground plane, perpendicular to the strip direction. The magnetic core can then be patterned into a rectangle with the long axis the same as the stripline direction. [55] This will give the magnetic film shape anisotropy with the easy axis along the stripline direction, and thus the hard axis perpendicular to this direction, in the same direction as the magnetic field. [18, 55] Microstrip lines have been demonstrated using both permalloy [18] and high-resistivity magnetic alloys [55]. In both cases, the inductors show significant inductance gain. By using magnetic alloys with high resistivity, the magnetic core can be deposited significantly thicker and an inductance gain of 11x was demonstrated (shown in figure 5b). [55] The microstrip inductors also have demonstrated high quality factor gain in the operating frequencies. [18, 55]

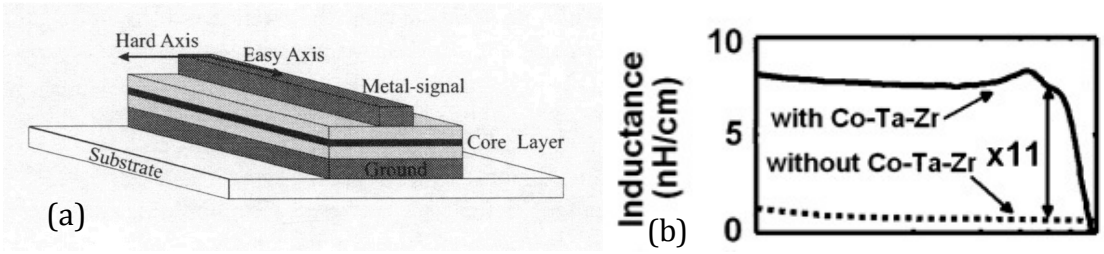

Figure 5: (a) Cross-section of a microstrip inductor with an integrated magnetic core layer and (b) the demonstrated inductance gain of a magnetic core inductor over an air-core microstrip using CoTaZr [55]

Spiral

The most often used inductor in current RF integrated chips is the planar spiral, shown in Figure 6a. [3] Since this is the design most often used, a well-established integrated fabrication process already exists and so the only fabrication challenge would be to incorporate the magnetic materials. [3] The spiral is intended to behave more like a solenoid than a strip inductor, with the inductance increase proportional to the square of the number of turns. [1] However, in practice it increases roughly linearly with the number of turns, behaving more like an elongated strip inductor. [1,3]

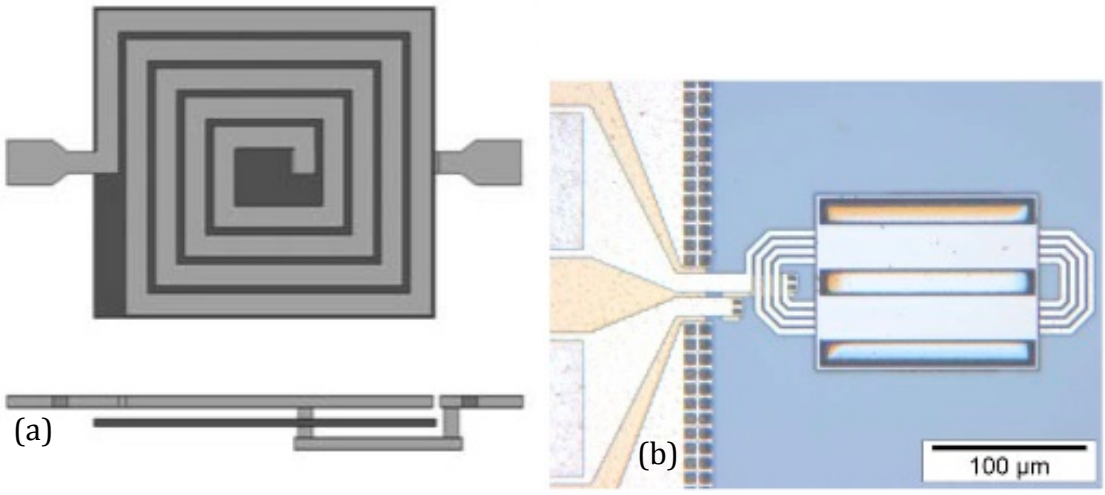

Figure 6: Spiral Inductor layout. (a) The often used square spiral with both top-down view and cross-section. (b) The use of an elongated spiral and two layers of magnetic material has been tested for increased inductance gain

Another challenge with spiral inductors is that the magnetic field is not in the same direction for each leg of the spiral. [23] The preferred axis for use in the magnetic inductors is the hard-axis and with a square spiral the hard axis needed for two different legs of the spiral will be perpendicular to each other (shown in figure 7b, as H_{ac}). [23] One of the options to solve this is to cover only half of the legs of the spiral with magnetic materials, effectively reducing the magnetic enhancement by 50% on a square spiral. [2] The spiral can be elongated (as shown in Figure 6b), which has been fabricated and shown, improving the total area covered by the magnetic material, but still below 100% coverage. [2] The third option would be to bias the magnetic material so that the easy-axis is out of plane, and therefore both in-plane axes would be a hard axis and show maximum inductance gain. Though perpendicular magnetization has been demonstrated in ultra-thin films [24-25], it is more difficult to achieve in an integrated core 100's of nm thick.

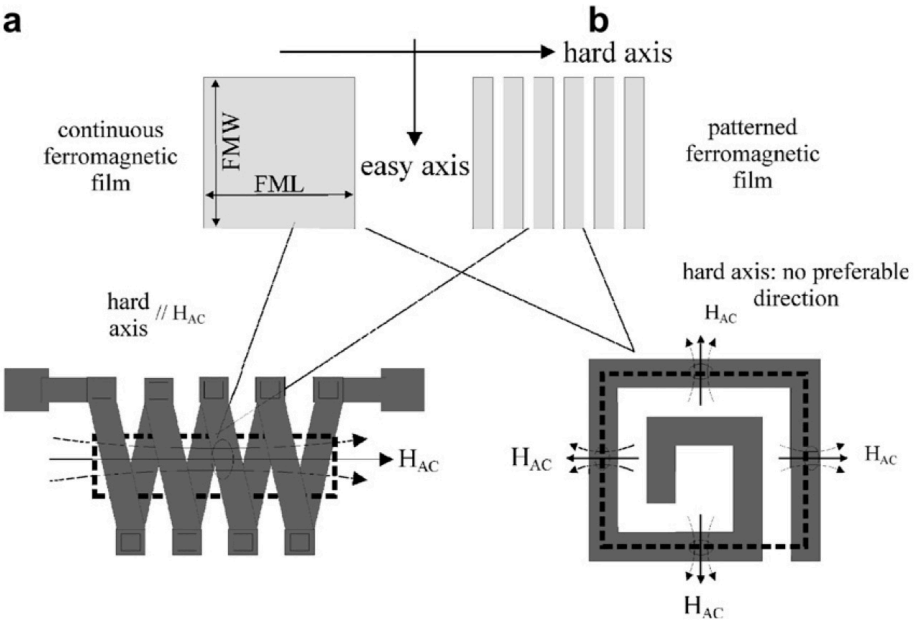

Figure 7: (a) An integrated solenoid design and the corresponding magnetic field in the core (H_{ac}). The hard axis operation of the core can be obtained by adding shape anisotropy. (b) Spiral inductor with the H_{ac} on different legs perpendicular to each other.[23]

With the inductance gains shown in the strip inductors, a magnetic film enhanced strip inductor can easily be fabricated to have equal or higher inductance as an air-core spiral inductor currently in use. This would ease the fabrication process and significantly reduce the density needed. Magnetic spiral inductors will need to be improved further with the integration of magnetic films to show high enough inductance gain to be used over magnetic strip inductors.

Solenoid

The potential for significantly higher inductance densities has increased the research into the integrated solenoid inductor. [11, 23] By using a solenoid type inductor, only a single magnetic film is required (compared to sandwich strips) and the magnetic field is entirely in the same direction (as compared to spiral type, shown in figure 7b). [23] The air-core solenoid type (shown in figure 8) has inductance gain proportional to the square of the number of coils, and has shown the significant magnetic enhancement when using magnetic cores. [11] Integration into CMOS fabrication is the most difficult challenge facing the solenoid type inductor because of increased fabrication complexity. [11, 23] It requires more lithography steps, significantly better alignment, and the addition of planarization steps in between layers, as compared to both the strip and spiral type inductors. [2, 23] However, the inductance gain is only limited to how thick the magnetic material can be made and how high the permeability is (as shown in equation 1). [11]

Another challenge with the solenoid type inductors is that the magnetic field (H_{AC} in figure 7) is along the easy axis of the core if it is patterned to fit in the solenoid as a single rectangle. [11, 23] One solution for this is to break up the core into smaller strips along the core, with only a small gap between them (shown in figure 7, top). This will

give the core a shape anisotropy such that the hard axis will be along the direction of H_{AC}, improving performance. [23]

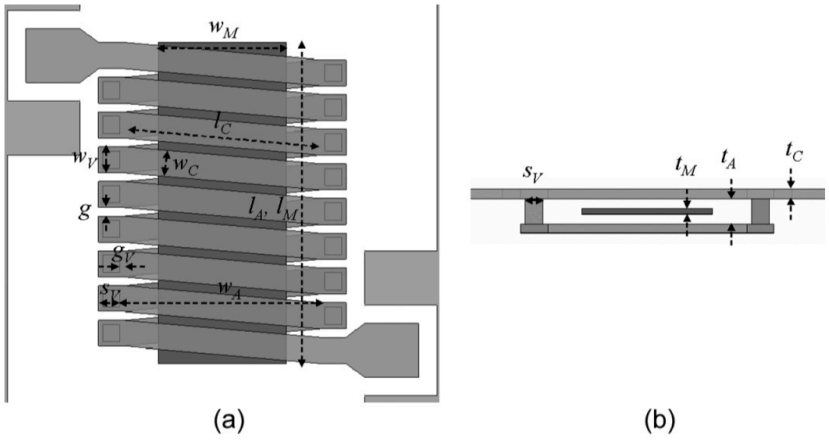

Figure 8: Solenoid design (a) top down view and (b) cross section view [11]

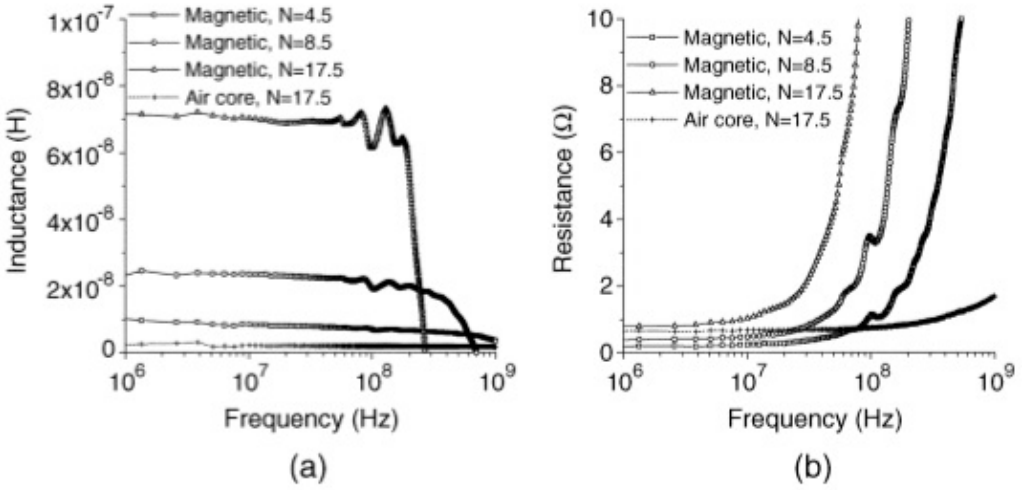

Figure 9: (a) Inductance vs. frequency and (b) resistance vs. frequency for different solenoid designs [11]

Solenoid devices have been fabricated using magnetic materials in the core and have shown significant inductance improvement. [11] Figure 9 shows the plot of both inductance vs. frequency and resistance vs. frequency for integrated solenoid devices. These plots show that even be reducing the number of coils by a factor of 4 (17.5 to 4.5),

by using a magnetic material, the inductance is still larger for 4.5 coils when compared to 17.5 with an air-gap. [11] This is a significant density improvement, and with better magnetic materials can be even larger.

Multiferroics

Background

A multiferroic is a material that exhibits at least two of the three ferroic properties: ferroelectricity, ferromagnetism, and ferroelasticity. [26] Multiferroics, specifically those that combine ferroelectricity and ferromagnetism (as shown in Figure 10), show promise in devices that use magnetism and have had an increase in research devoted to them in recent years. [26-27] Many devices that utilize magnetic films have been demonstrated to be useful and adjustable with applied external magnetic fields. [1-3] However, in real applications it is not desirable nor energy efficient to need to apply a magnetic field to a device for it to work. For this reason multiferroics have been investigated in hopes of utilizing an electric field to adjust magnetic properties so that devices can be both integrated and energy efficient, showing promise in many different low-energy applications. [26-28]

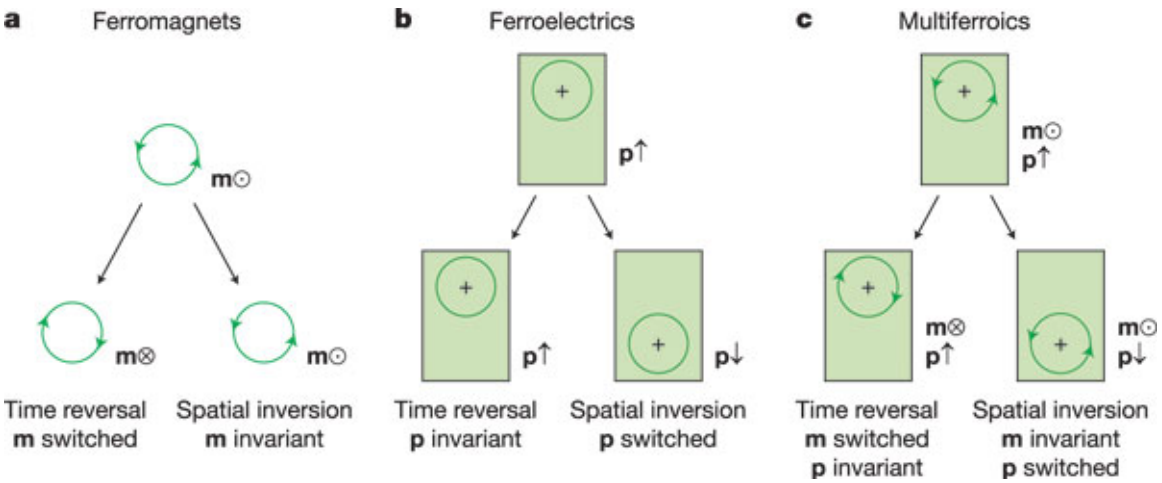

Figure 10: Comparison of the effect for (a) ferromagnetic materials, (b) ferroelectric materials, and (c) multiferroics combining the two [26]

There are three main configurations multiferroics have been fabricated in for use in devices, all depicted in figure 11. [27] Growing multiferroic materials on single crystal substrates, shown in figure 11a, has been demonstrated but has shown poor coupling between electric field and magnetic properties. The existence of both ferroelectric and ferromagnetic properties in the same material is extremely rare because the mechanism for ferroelectricity (cation off-centering, which requires empty d-orbitals) and ferromagnetism (which usually results from partially filled d-orbitals) both use different occupation of d-orbitals. [27] Therefore, for both properties to exist in the same material, the atoms that move off center for ferroelectricity need to be different than the atoms that carry the magnetic moment. [27] This has been achieved by finding materials with an alternative mechanism for ferroelectricity, though there is also the possibility of finding materials with alternative forms of ferromagnetism. [27]

The more promising multiferroics have been demonstrated using heterogeneous structures, shown in figure 11 (b) and (c). [27] Two-phase multiferroics use a coupling mechanism between a ferroelectric and ferromagnetic material to get an effective coupling between electric and magnetic fields. [26-28] The most commonly used coupling mechanism so far has been strain. These multiferroics combine a piezoelectric material (electric field to strain) with a magnetostrictive material (strain to magnetic field) to obtain the multiferroic effect (electric field to magnetic field). [26-28] With such hetero-structures, single-crystal substrates are not necessarily needed for film growth and significantly stronger coupling has been demonstrated. [26] The structures most often used are the horizontal layering, like figure 11b. Though they are usually more difficult for fabrication, vertical hetero-structures offer many advantages. The vertical structure (such as nano-pillars) will have larger interfacial surface area between the ferroelectric and ferromagnet, increasing coupling. One of the major challenges of horizontal

structures is the substrate-imposed mechanical clamping, which vertical structures will not eliminate. [27]

Figure 12 below shows a plot of the different magneto-electric (ME) coefficients for both single phase and two-phase multiferroic systems. [28] The single-phase systems are generally measured at low-temperature while the two-phase ones are measured at room temperature. [28] Even with this temperature difference, the two-phase systems have orders of magnitude better coupling. [26-28]

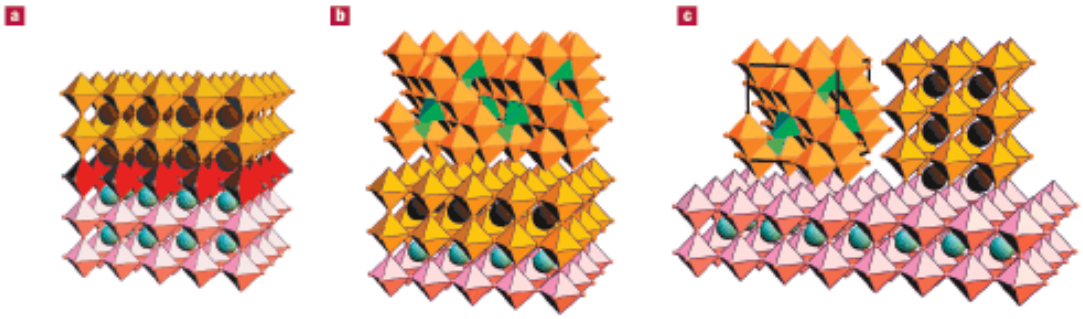

Figure 11: The three main multiferroic structures: (a) epitaxial grown multiferroic films on single crystals, (b) a ferroelectric film deposited with a ferromagnetic film on top, coupled through strain, and (c) a ferroelectric film deposited next to a ferromagnetic film, coupled through strain. [27]

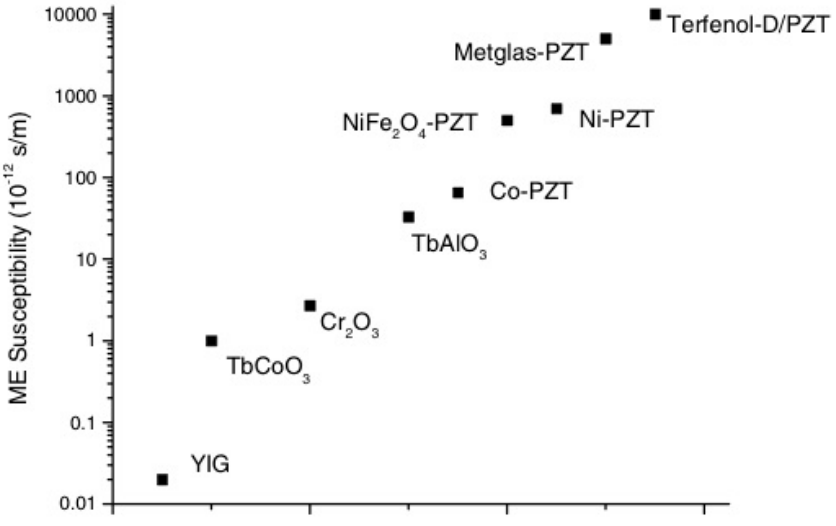

Figure 12: The maximum experimentally demonstrated ME susceptibility for different multiferroics, both 1- and 2-phase. The 2-phase show the maximum at room temperature while the 1-phase systems are generally at low temperatures. [28]

Material Properties

Since multiferroic designs that utilize a strain mediated coupling have shown the strongest effects so far, the materials considered will be limited to these choices. The most common choice of materials for these multiferroics is to utilize a ferroelectric material with a ferromagnetic material. [26-28] In order for the coupling between the two materials to be strong, the ferromagnetic material needs to have a strong magnetic response to any strain it experiences (called magnetostriction). [26-28] When making two-phase systems, the two ferroic materials will need to be in close contact with each other to make sure that the coupling will be maximum. [26-27] Since the coupling is strain mediated, it is better if there are no materials between the two ferroics and that there are no defects in the materials, so that the strain will not be dissipated, weakening the coupling. [28] The magnetoelectric coefficient, $\alpha_{ME}=\Delta H/\Delta E$, is a measure of the coupling between the magnetic and electric fields, and the larger the piezoelectric coefficient (e-field to strain) and magnetostriction coefficient (strain to magnetic field), the larger α_{ME} can be. [29]

The piezoelectric and magnetostriction coefficients are not the only consideration when making a device, but also the frequency that the voltage will be applied is important. [28] The α_{ME} of the system will have a strong dependence on the applied AC voltage frequency, peaking when there is a resonance between the ferroelectric and ferromagnetic materials. [28] This is shown in figure 13 below, where the α_{ME} of a two-phase system of Ni/PZT(lead zinc titanat)/Ni is measured versus frequency of the applied AC voltage. [28] The plot shows a large peak at the resonant frequency (~200 times normal value), and this resonance can be tuned to a desired frequency by selection of materials. [28]

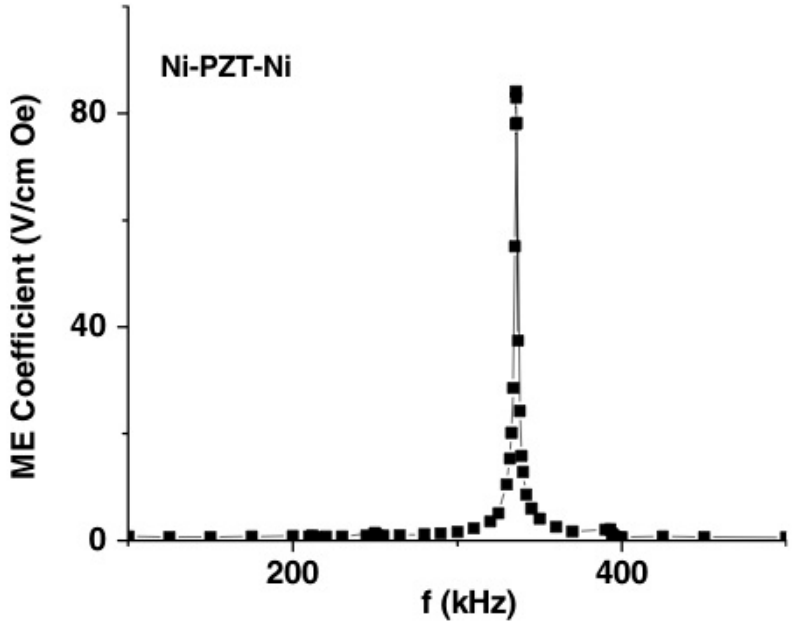

Figure 13: ME Coefficient vs AC frequency of Ni-PZT-Ni two-phase multiferroic, showing the resonance peak which improves the ME coefficient by about 200 times. [28]

Two-Phase Systems

Many different two-phase systems have been studied for stronger α_{ME} and for different applications. [26-29] Table 2 below shows the important properties of a few common ferroelectric and ferromagnetic materials that can be combined to form a two-phase multiferroic. [26-29] Some two-phase systems have been made to alter the magnetization of the ferromagnet and some are made to alter the magnetic structure. [26] One that alters the magnetization used FeGaB films deposited on single crystal PZN-PT (lead zinc niobate-lead titanate) to form a multiferroic. An electric field was applied across PZN-PT and the FMR resonance of FeGaB was measured at different values using spin-wave resonance, with a measured change in frequency equivalent to when 750 Oe is applied to the film. This corresponds to a α_{ME} of approximately 94 Oe-cm-kV^{-1}. [29] Another group used a $BaTiO_3$ (BTO) substrate with an epitaxial

$La_{0.67}Sr_{0.33}MnO_3$ ferromagnetic film. Applying a voltage across the substrate, the measured magnetization could be changed up to 70% at room temperature. [30] One of the attempts at altering the magnetic structure used a PZN-PT substrate with NiCo thin film. With patterned films, the E-field was strong enough to rotate the magnetization by 90°, and with a GMR structure the strain was strong enough to rotate the magnetization a complete 180°. [31] Similarly, another group demonstrated 90° rotation of the magnetization using a ferroelectric lead zirconate titanate (PZT) film with a ferromagnetic CoPd thin film. [32]

Ferroelectric	Piezoelectric Coefficient (pC/N)	Ferromagnetic	Magnetostriction Coefficient (ppm)
ZnO	11	YIG	2
BTO	100	CoFeB	15-30
PZT	200	Ni	20-50
PZN-PT	2200	GaFeB	60
PMN-PT	1000-1800	Terfenol	1600

Table 2: Ferroelectric and Ferromagnetic materials that are often used in 2-phase multiferroics

Device Applications

Multiferroics show promise for many different device applications, and with improving α_{ME} coefficients from two-phase systems, will be able to be utilized in many different areas. [26-32] Devices that use the properties of multiferroics have shown promise in areas such as ultra-sensitive magnetic field sensors, energy storage, energy harvesting, magnetic recording devices, and electric and magnetic field tunable microwave devices. [28] The multiferroic devices being investigated for use as ultra-sensitive magnetic sensors are promising for use similar areas as SQUID is currently used. The multiferroic devices have shown to have as high a sensitivity, but more importantly they are simpler to fabricate and are functional at room temperature, removing the need of liquid helium SQUID has. [26, 33] Multiferroics are also being

investigated for unique optical properties. A two-phase multiferroic using PZT placed a magnetic garnet between two cross polarizers. When the electric field is applied to PZT, the Faraday rotation of the garnet is affected and gives the device controllable optical transmission. [34]

Another device application that has been explored is combining giant magnetoresistance (GMR) structures with ferroelectric substrates or films. The GMR structure used was FeMn/$Ni_{80}Fe_{20}$/Cu/Co/PZN-PT(Substrate). [31] These magnetic multilayers ensure that when using E-field, the bottom bit will act as the free layer since Co has the largest magnetostriction of any element, and the NiFe layer will not change magnetization because it has no magnetostriction. Using the E-field tuning of the two-phase multiferroic, the magnetization of the GMR bit can be rotated a complete 180°. This switching using E-field (shown below in Figure 14) is potentially more energy efficient than using either current or magnetic field and shows promise for low energy magnetization reversal. [31]

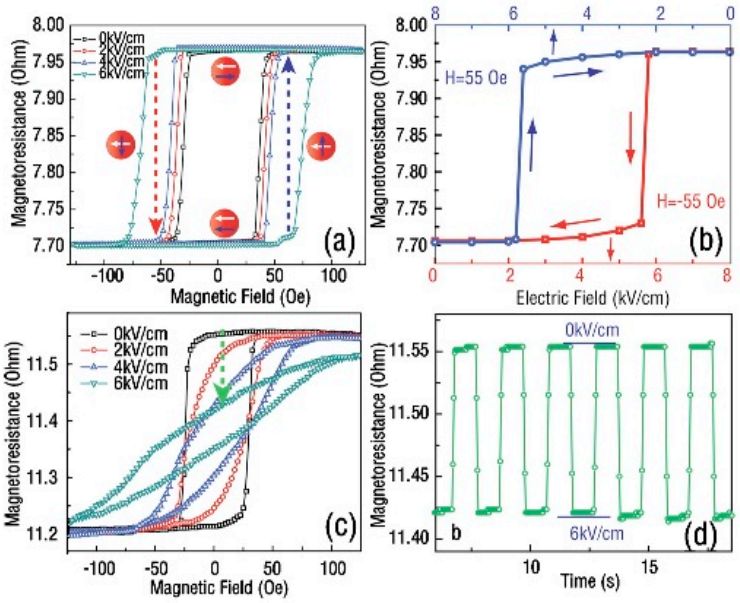

Figure 14: Switching of a GMR bit using an applied E-Field. Complete 180° switching of the magnetization is demonstrated, showing the same resistance values for E-field switching in (b) as is seen for magnetic field switching in (a) [31]

Non-volatile Devices

A recent study has shown that there is potential for non-volatile multiferroics, as well. By combining a ferroelectric that exhibits a strain hysteresis with a magnetostrictive ferromagnetic material, the magnetic change can remain even after the voltage is removed from the ferroelectric. [35] This has promise for use in low energy devices that can be tuned with a voltage and then have the voltage removed during operation.
The two-phase system that demonstrated the non-volatile multiferroic used lead magnesium niobate-lead titanate (PMN-PT) as the ferroelectric substrate and Ni as the ferromagnetic film. The substrate used is the (110) direction, which has anisotropic strain and shows a large peak in strain when the voltage is slowly swept in the opposite direction of the poling voltage. If the voltage sweep is stopped before passing this strain peak, the strain will remain even when the electric field is removed. This large strain peak and resulting hysteresis are shown in figure 15 below. The red curve is the full voltage sweep, while the blue curve shows the hysteresis when the sweep is stopped before passing the strain peak. [35]

The strain hysteresis comes from the reversal of the polarization when going from positive to negative electric fields. [35] When the PMN-PT is poled along the positive direction, the polarization will be along the [110] direction (shown in figure 16). This will exert an anisotropic strain with positive strain along the Y-axis and negative along the X-axis. In order for the polarization to reverse, the polarization will travel along [110] direction towards [$\underline{1}10$]. Near an E-field of 1.4kV/cm (opposite the poling direction), the strain will become positive in both the X and Y-directions as the polarization reverses (shown in figure 16, inset). This reversal will cause the large strain, and if the E-field is

not increased, the PMN-PT polarization will remain in this metastable state, resulting in the strain hysteresis. [35]

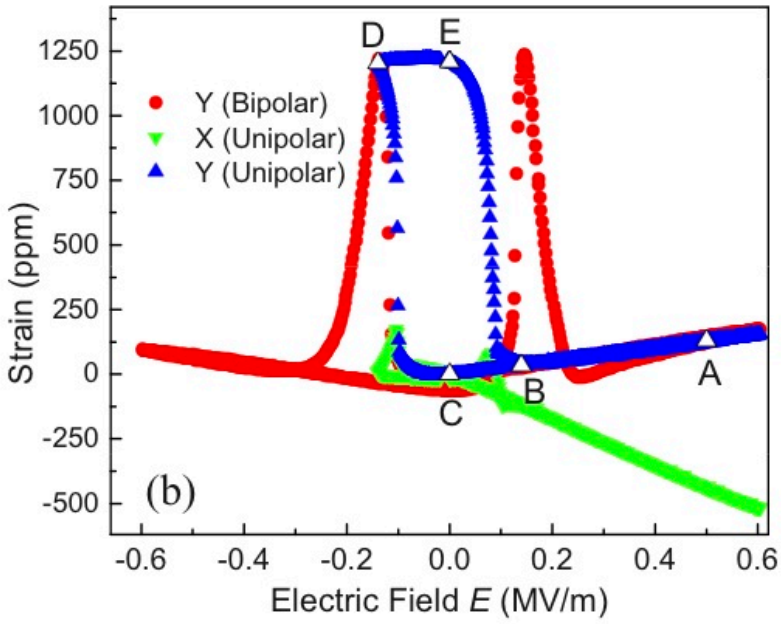

Figure 15: Strain hysteresis seen in <110> PMN-PT. The red curve shows the full sweep of the strain from poling at 0.5MV/m to re-poling at -0.5MV/m. The blue curve shows the hysteresis that can be formed by stopping the voltage sweep before passing the strain peak at -0.14 MV/m [35]

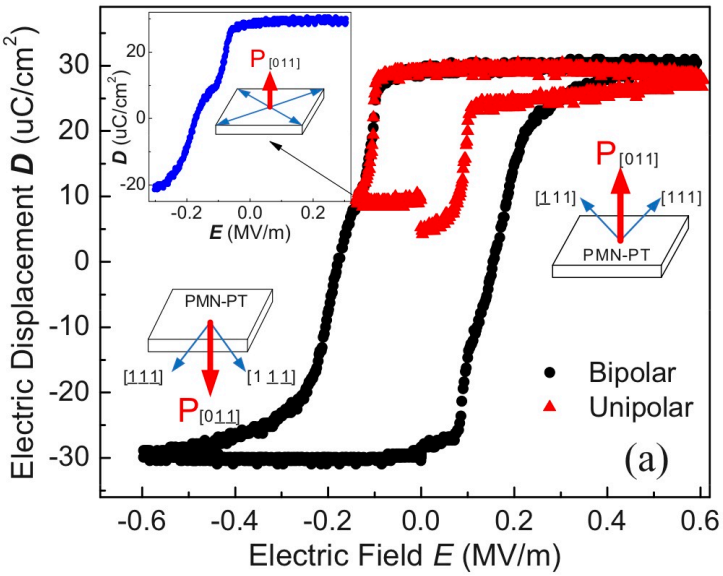

Figure 16: Electric Displacement of the PMN-PT substrate under applied Electric Field. The displacement is depicted on the graph, with the inset showing the polarization reversal that causes the large strain, resulting in the strain hysteresis. [35]

By depositing a Nickel thin film onto a (110) PMN-PT substrate, the group created a multiferroic system. The magnetostriction of Ni is one of the highest for a single element (only Co is higher) and so the α_{ME} has been shown to be strong in this two-phase system. [35] Applying a sequence of voltages similar to those shown in the blue curve of figure 15, a non-volatile change in the magnetism of the nickel film can be seen. A magneto-optical Kerr effect (MOKE) measurement was performed on the Nickel film to demonstrate this effect and the results are shown in figure 17. [35] The linear change is seen when decreasing the applied E-field from poling (0.5MV/m) to 0. The strain peak E-field is applied (-0.14 MV/m) and then removed, and the magnetic hysteresis curve is nearly identical. [35] The strain peak shows a strong effect on the Ni film, rotating the magnetization from an easy-axis to almost a hard-axis measurement with just the E-field. [35]

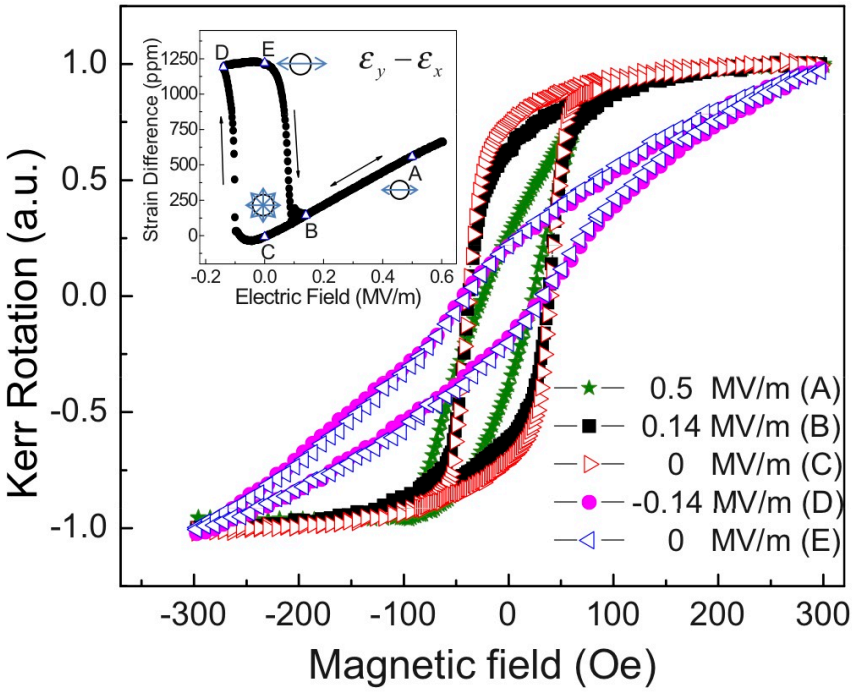

Figure 17: Magnetic hysteresis measured by MOKE of Ni thin film on PMN-PT <110> for different applied electric fields. The PMN-PT is poled at 0.5 MV/m and then the strain hysteresis (shown in the inset) is used to obtain a non-volatile change in the Ni film [35]

Voltage Tuned Inductors

Inductances that utilize a magnetic film can easily be tuned using an applied magnetic field, but this is not energy efficient nor is it useful for individually tuning devices in an entire circuit for optimum performance. [1-3] For this reason, electrically tunable inductors have been investigated.

Tunable Device Structures

Some of the first voltage tunable inductors had discrete tuning using switches (MOSFET or MEMS) between multiple inductor coils. [36-39] If the switches are open, the inductance is only the value of a single coil, and with each closed switch the inductance of another coil is added. This allows tuning between a few different inductances with potentially large inductance tuning (>1000%)[37] but only between different discrete inductances. This can be useful in applications that need to switch between 2 or 3 different frequencies for LC circuits, but not for fine tuning to any desired frequency on a continuous spectrum. [36-39]

For continuous tuning of the inductance, there have been many different proposed and demonstrated structures. [5, 13, 40-54] One structure uses a high-conductivity metal for the inductor with a low-conductivity material effectively coiled around the inductor (shown in figure 18a). [42] By passing a current through the coiled material, a DC magnetic field is effectively applied to the inductor, tuning the devices inductance. [42] This uses the applied magnetic field method of tuning inductors but makes it possible to tune individual inductors, though it still uses current for tuning and so is not very energy efficient. It has only been demonstrated with moderate tuning range using a tuning current of 15mA (18% at 5MHz, up to 80MHz operation). [42] Continuous tuning has also been investigated by using core displacement (depicted in

figure 18b). [5, 43-44] By displacing a ferromagnetic core in the inductor, the inductance can have a wide tuning range, up to 400% has been demonstrated. [43] This has been done using MEMS devices (silicon microgrippers, sockets, and handles) to displace a NiFe core and enhance the inductance from its initial value of 5.5nH. [43] Other groups have used the core displacement concept with MEMS, but have used fluid cores instead for easier displacement and finer tuning control (shown in figure 18c). [5] The fluid is ferromagnetic and therefore an actuation coil, removing the need for any mechanical motion, can control the displacement. Using a planar spiral design and displacing the ferrofluid with the actuation coil can tune the inductance by 16% [5]

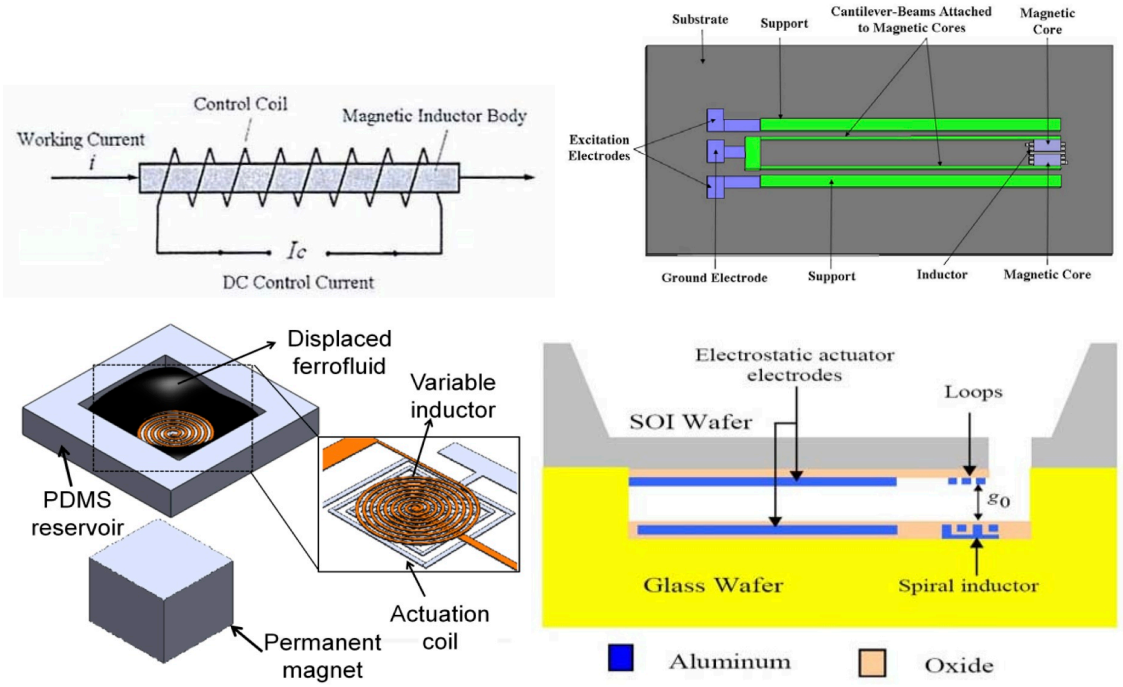

Figure 18: Different MEMS structures that have been used for continuous inductance tuning range. (a) An inductor with high conductivity metal with a lower conductivity metal surrounding it, creating an effective field with DC current I_c. (b) Design of a core displacement using electric actuation for control. (c) A core displacement design using a ferrofluid and an actuation coil for control over the displacement. (d) A design for an inductor that uses mutual inductance for tuning. A voltage between the actuator electrodes will bend the cantilever, changing the distance between loops, and thus the mutual inductance.

The MEMS type inductors have demonstrated variable inductance, but there are still many challenges with them. Many of them still use current driven tuning, have very complex fabrication, or use mechanical motion, which has potential for wearing down. [40-51] Another tuning method that has been investigated is using multiferroics to adjust the permeability of a magnetic film. [13, 52-53] If it is integrated into a magnetic film inductor, this change in permeability will change the inductance. This method would allow for continuous tuning and it would be very energy efficient because it uses voltage, not current. [13, 52-53] One of the first successful attempts at using magneto-electric coupling used a magnetic toroid core, with a PZT slab placed in the center (figure 19a). [52] When a voltage is applied to the PZT, the strain will change the permeability of the ferromagnetic core, tuning the inductance. Using this method, the device had a tuning range of ~20%, but low operation frequency (kHz range). [52] Another group also used a toroid ferromagnetic core, but deposited PZT directly onto the ferromagnetic on both sides (figure 19b). The electric field is applied to the PZT and should provide improved coupling between the PZT and ferromagnetic core. The tuning range increased to over 50% (56.6% at the peak) and the operation frequency was significantly improved by an order of magnitude. [53]

Another group to have demonstrated this type of tuning also used PZT with ferromagnetic material as a solenoid core. Taking a PZT substrate, Metglas 2605CO™ was deposited on both sides and the entire substrate was used as the core (figure 19c). [13] Using this device, electric field controlled tuning was demonstrated with tuning range >400%, with an operating frequency approaching 1MHz. [13] The multiferroic approach shows promise for a large continuous range, but they have only been demonstrated in the kHz frequencies as discrete, not integrated, devices. [13, 52-53] A summary of the different variable inductors, including the method of tuning, is given below in table 3. [5, 13, 36-54]

Initial Inductance	Tuning Type	Tuning Range	Quality Factor	Actuation Needed	Tuning Method	Maximum Frequency	Reference
8 nH	Discrete	200%	7	1.6 V	Series Inductors	2 GHz	[36]
2.5 nH	Discrete	1000%	-	20 V	Series Inductors	-	[37]
9.5 pH	Discrete	50%	19	-	Series and Parralel Inductors	10 GHz	[38]
1.1 nH	Discrete	47%	20-45	40V	Magnetic Coupling Coefficient	6 GHz	[40]
1.83 nH	Continuous	42%	12	1.2V	Permeability Change	2 GHz	[41]
-	Continuous	18%	17	15 mA	Magneto-impedance	80 MHz	[42]
5.5 nH	Continuous	400%	50	7V	Core Displacement	10 GHz	[43]
0.245 nH	Continuous	31%	5.6	86.2 V	Core Displacement	8 GHz	[44]
0.5 nH	Continuous	100%	26	10 mW	Magnetic Coupling Coefficient	25 GHz	[45]
0.748 nH	Continuous	30%	24.3	155 mV	Magnetic Coupling Coefficient	7 GHz	[46]
1.185 nH	Continuous	13%	-	-	Magnetic Coupling Coefficient	-	[47]
1.69 nH	Continuous	294%	8.83	140V	Magnetic Coupling Coefficient	25 GHz	[48]
2.65 nH	Continuous	108%	17	-	Current Loop Area	100 MHz	[49]
2.2 nH	Continuous	100%	27	-	Magnetic Energy Stored	8.3 GHz	[50]
1.5 nH	Discrete	200%	4	55-60V	Series Inductors	25 GHz	[51]
450 µH	Continuous	20%	-	5 kV/cm	Multiferroic	10 kHz	[52]
1 mH	Continuous	57%	-	3 kV/cm	Multiferroic	100 kHz	[53]
0.2 mH	Continuous	400%	8	12 kV/cm	Multiferroic	1 MHz	[13]
-	Continuous	35%	-	-	Synthetic Antiferromagnet	800 Hz	[54]
0.678nH	Discrete	55%	7	1.5 V	Series Inductors	3.4 GHz	[4]
220 nH	Continuous	16%	24	1.2 A	Core Displacement Ferrofluid	50 MHz	[5]
5.4 nH	Continuous	107%	12	-	Micro-fluid Coupling	1.6 GHz	[39]

Table 3: Summary of different tunable inductors and the tuning method used. – indicates the value for that device could not be found

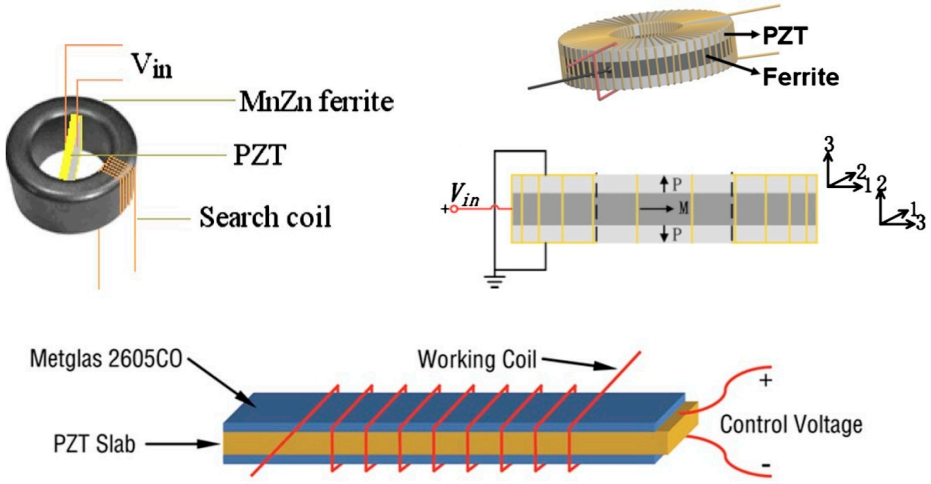

Figure 19: Multiferroic materials incorporated into inductors for electric field tuning, using the multiferroic as the inductor core. (a) Uses a ferrite toroid with a PZT slab in the middle, (b) uses a ferrite toroid with PZT deposited on both sides, and (c) uses a PZT slab with Metglas 26050CO bonded to both sides.

Multiferroic Device Design and Fabrication

Design

For the design of the inductor, the choices are similar to magnetic film inductors previously described (strip, spiral, or solenoid). Since the solenoid design would encapsulate the core and pose fabrication challenges with integrating the multiferroics, that design was ruled out. The spiral inductor would not be ideal since the piezoelectric substrate would exert anisotropic strain, so the potentially perpendicularly oriented magnetic films would have different changes in magnetization. [23] Therefore, the device design chosen was a microstrip inductor, since it has one of the simpler fabrication processes and has already been demonstrated to have high inductance gain with magnetic films. [18, 55] The downside of the microstrip inductor is that there will have to be a ground plane and isolation oxide layer between the ferromagnetic core and ferroelectric substrate, reducing the coupling. Keeping these layers to the minimum

thickness and using a substrate with a high piezoelectric coefficient, such as PMN-PT, can overcome this.

The magnetic core material will be more difficult to choose. Most magnetic materials discussed earlier that are good for magnetic film inductors will not work for E-field tuning. [1-3] One of the requirements for general magnetic film inductors is that the ferromagnetic material has low or no magnetostriction so that stresses during fabrication will not alter the magnetic properties. [2] For E-field tuning, a high magnetostriction is required to have high coupling for the multiferroic. [26-27] There are two options for making the magnetic core: a new magnetic material can be found that will have high permeability but also high magnetostriction, or a bilayer can be used for the core with one layer having high magnetostriction and one layer having the other desired magnetic properties (high M_s, high resistivity). The latter was chosen for these initial devices for the ease of fabrication. Nickel, a metal with strong magnetostriction [28], and $Ni_{80}Fe_{20}$ (permalloy), an alloy with high permeability and moderate resistivity, are readily available and easily deposited for integrated devices. [18] Based on other bilayer experiments and simulations, the Ni/NiFe bilayer magnetic properties will be a linear combination of the two based on thickness. [56] With the control over thickness, a balance can be tuned between the strong magnetostriction but poor permeability of Ni with the weak magnetostriction but high permeability of NiFe. The thicknesses chosen for this balance of properties were 40nm of Ni with 120 nm of NiFe (1:3 ratio for Ni:NiFe).

Calculation of Device Characteristics

Using the linear approximation for the properties of the bilayer, the important device characteristics can be calculated for comparison after fabrication and are given below in table 4. The tuning range can be approximated by calculating the change in

permeability caused by the strain of the PMN-PT. An effective field can be calculated from the PMN-PT properties and Ni magnetostriction (equation 7) and H_{ME} will effectively replace $H_{external}$ in equation 3. These values are then used in equation 2 to give an approximation for the E-field tuned permeability (equation 8). The measured permeability for device applications will be different than the theoretical value, so the tuning range is estimated by the percentage change calculated.

$$H_{ME}=\frac{3\lambda_s Y d_{31} E}{M_s} \quad (7)$$

$$\mu=\frac{4\pi M_S}{1+H_a+\frac{3\lambda_s Y d_{31} E}{M_S}} \quad (8)$$

The FMR frequency calculated for the thin film bilayer used in these devices is more complicated than the bulk equation given in equation 4. The demagnetization fields will affect the FMR frequency and can be estimated using equation 9. [60] Each demagnetization field can be calculated by rotating which variable is given the dimension value (c->a->b->c) and repeating the calculation three times. [61] Taking into account the demagnetization for the FMR frequency is given by equation 10. [61] This gives a FMR frequency less than eddy current loss frequency, which means there should not be significant eddy current losses in these inductors.

$$\begin{aligned}\pi D_z=&\frac{b^2-c^2}{2bc}\ln\left(\frac{\sqrt{a^2+b^2+c^2}-a}{\sqrt{a^2+b^2+c^2}+a}\right)+\frac{a^2-c^2}{2ac}\ln\left(\frac{\sqrt{a^2+b^2+c^2}-b}{\sqrt{a^2+b^2+c^2}+b}\right)+\frac{b}{2c}\ln\left(\frac{\sqrt{a^2+b^2}+a}{\sqrt{a^2+b^2}-a}\right)+\frac{a}{2c}\ln\left(\frac{\sqrt{a^2+b^2}+b}{\sqrt{a^2+b^2}-b}\right)\\&+\frac{c}{2a}\ln\left(\frac{\sqrt{b^2+c^2}-b}{\sqrt{b^2+c^2}+b}\right)+\frac{c}{2b}\ln\left(\frac{\sqrt{a^2+c^2}-a}{\sqrt{a^2+c^2}+a}\right)+2\arctan\left(\frac{ab}{c\sqrt{a^2+b^2+c^2}}\right)+\frac{a^3+b^3-2c^3}{3abc}\\&+\frac{a^2+b^2-2c^2}{3abc}\sqrt{a^2+b^2+c^2}+\frac{c}{ab}(\sqrt{a^2+c^2}+\sqrt{b^2+c^2})-\frac{(a^2+b^2)^{3/2}+(b^2+c^2)^{3/2}+(c^2+a^2)^{3/2}}{3abc}.\end{aligned}$$

$$f_{FMR}=\frac{\gamma}{2\pi}\sqrt{(H_a+(D_x-D_z)M_S)\cdot(H_a+(D_y-D_z)M_S)} \quad (10)$$

M_S	Magnetostriction	Resistivity	FMR frequency	Eddy Loss Frequency	Tuning Range
0.9 T	20 ppm	30 μΩ cm	1.8 GHz	3.8 GHz	12.4%

Table 4: Calculated magnetic properties for Ni(40nm)/NiFe(120nm) core

Fabrication Process

The fabrication starts with a PMN-PT substrate, cut with the (110) orientation to obtain the strain hysteresis. [35] The ground plane electrode is first deposited using E-Beam evaporation (with a CHA Solution Electron Beam Evaporation System). Aluminum is deposited (150nm) with a 100nm thick Silicon Dioxide layer deposited in-situ on top to insure isolation between the ground plane and magnetic core. Using a lift-off process, 40nm Ni is deposited using E-Beam evaporation and 120nm NiFe is sputter deposited (using ULVAC JSP 8000 Sputter System). A thick oxide is deposited using PECVD (using a STS MESC MULTIPLEX CVD) over the entire substrate, isolating the magnetic core from the top electrode. Vias are etched (using a STS MESC MULTIPLEX Advanced Oxide Etcher) through both layers of oxide to reach the bottom Al film. A thick layer of Al is sputter deposited (after an in situ Ar sputter etch to ensure a good contact between the ground plane and top electrode) and then patterned by Cl_2 etching (using a Unaxis SLR770 ICP). Finally, the back electrode is deposited using e-beam evaporation of Cu. During the back electrode deposition, the devices are protected by a spin-on resist (AZ5214) to ensure the devices are not damaged. The entire fabrication process is depicted in figure 20. Also shown in figure 20 below is the completed cross-section view and completed top-down view of the inductors. The measured inductors were shorted to the ground plane at one end and had GSG pads at the measurement end. To make sure a good electrical connection was made, resistance measurements were performed between all the ground pads.

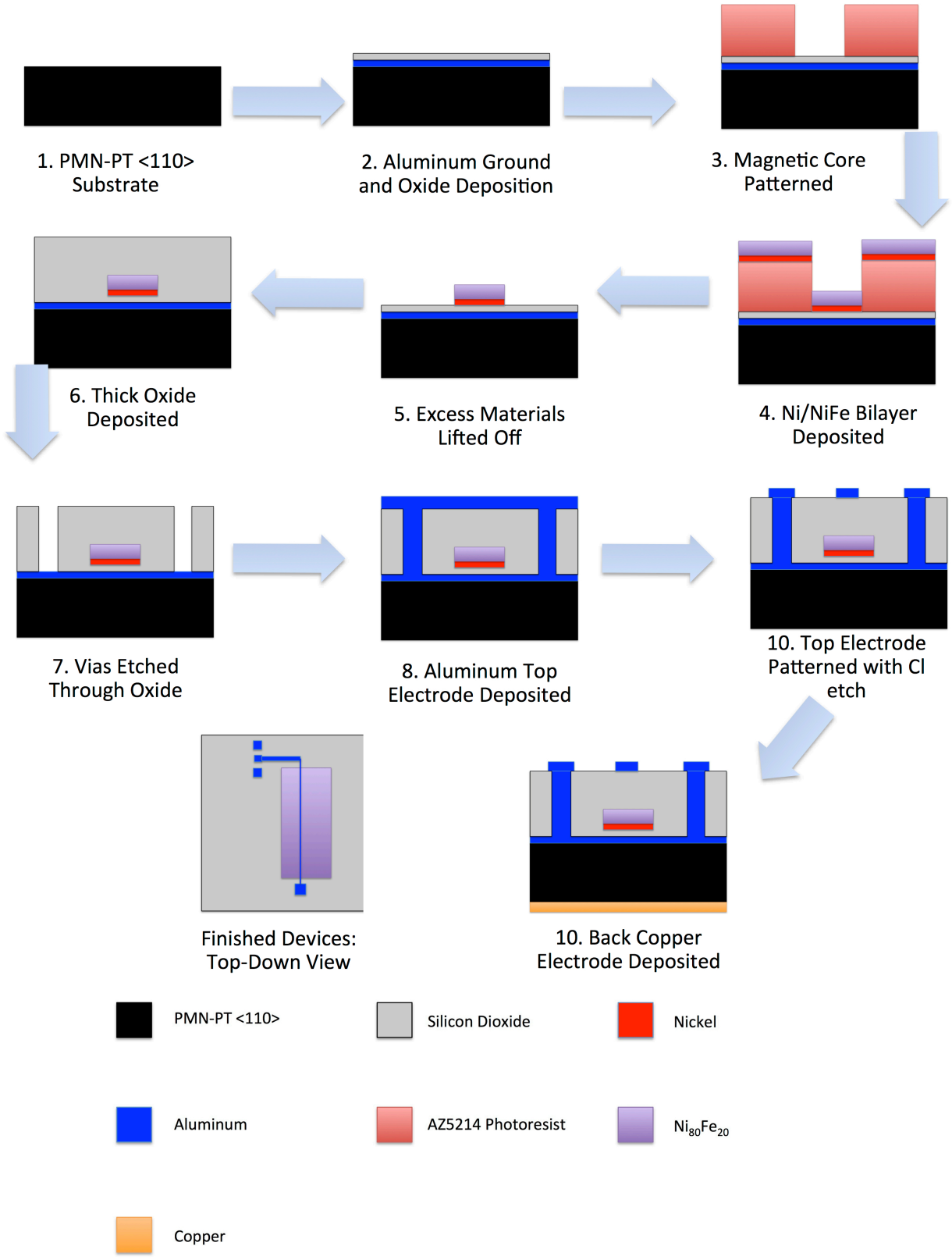

Figure 20: Fabrication process flow for microstrip inductors (images not to scale).

Results and Discussion

The microstrip inductors were characterized by using a network analyzer to obtain 1-port scattering parameters (S-parameters). The S-parameters are then converted to impedance to get the inductance value versus frequency for different applied E-Fields. An external magnetic field was applied along the easy axis to measure the tuning range in different external fields and to characterize the magnetic core. The equations used for converting from S-parameters to impedance and then to inductance and quality factor are:

$$Z = Z_0 \cdot \frac{1+S_{11}}{1-S_{11}} \quad (6)$$

$$L = \frac{\mathrm{Im}(Z)}{2\pi f} \quad (7)$$

$$Q = \frac{\mathrm{Im}(Z)}{\mathrm{Re}(Z)} \quad (8)$$

The inductors were first measured and compared to devices made with the same process but with no magnetic core. The plot of inductance for with and without a magnetic core is shown below in figure 21. The inductance enhancement at GHz frequencies is ~75% change from regular inductors to magnetic film ones. This is less than expected with the high permeability of NiFe, but at high frequencies there are many loss mechanisms, which can account for this. Figure 21 shows the scattering parameters of the magnetic film inductors, revealing a very broad FMR peak. As was discussed in an earlier section, this will lead to high losses at frequencies near the FMR.

Another parameter that is an important measure for an inductor is the quality factor (Q). [1-3] The quality factor is the ratio of the reactance to the impedance of the inductor, and is a measure of its efficiency. [1] The higher the quality factor, the better the inductors performance will be, and to be useful in a circuit, the quality factor needs to

be greater than 1. [2] Magnetic thin films are not only used to enhance the inductance, but also the quality factor and have often shown improved Q as well as inductance. [1-3, 36-54] The magnetic films improvement of Q arises from the increase in reactance cause by the permeability increase, but a decrease in resistance would also result in an improved Q. [1-3, 59] One group used magnetic films layered with Cu to improve the high frequency resistance of the inductor, significantly increasing the Q at high frequency. [59] This was achieved by using the anti-ferromagnetic resonance of the NiFe layers to obtain a negative permeability for the magnetic layers. The interactions between the conducting layers and magnetic layers permeability will then result in very high conductivity at high frequencies, significantly improving the quality factor. [59]

For the microstrip inductors, the Q of the air core devices was very low to begin with (~0.5 at 1 GHz), so they would not be useful in an actual circuit. By adding the magnetic core, the quality factor was increased by a factor of almost 3 (to 1.4). This increase raises the quality factor over the minimum threshold for useful applications and shows improvement by 170%. The quality factor is also controlled by the applied E-field, and this control (as well as the quality factor enhancement) is shown in figure 22 below. The quality factor for the magnetic core devices has a peak just before the FMR frequency. At the FMR frequency, the quality factor approaches and equals the air-core quality factor, before increasing again. Since the quality factor is a measure of the device efficiency, the device will perform best when operated at a frequency near the peak Q. For this reason, the FMR frequency will need to be designed so that it is larger than the operating frequency, aligning the peak Q with device operation for optimal performance. This can be achieved during device design, or later by tuning with an external magnetic field or with an applied E-field.

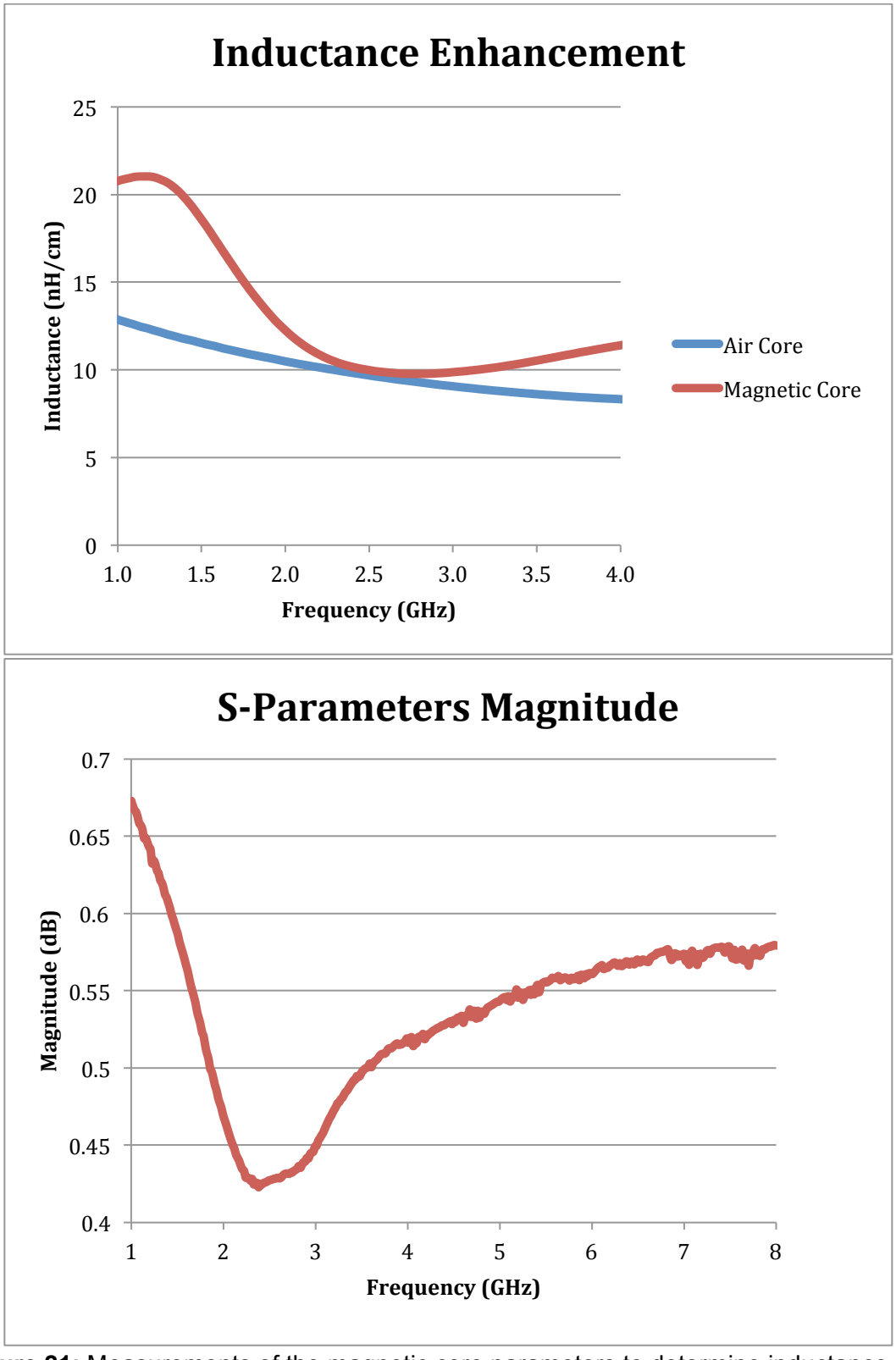

Figure 21: Measurements of the magnetic core parameters to determine inductance enhancement. (a) A plot of the inductance vs. frequency for identical devices for air core and magnetic core. (b) Plot of the magnitude of the measured S-parameters, showing a broad FMR peak

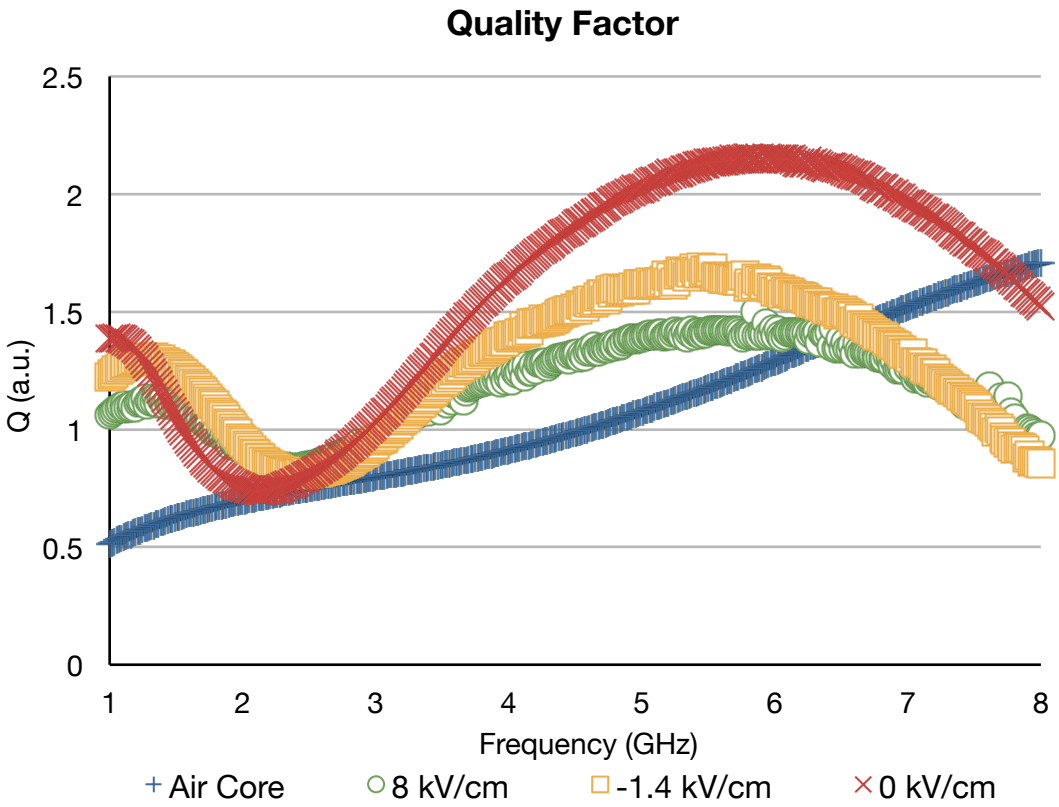

Figure 22: Quality factor of the inductors, comparing air core the magnetic core devices. Tuning of the quality factor using the E-field is also demonstrated

The inductor tuning was measured first with no external magnetic field. The measurements were performed after poling the PMN-PT substrate at a positive 400V (8kV/cm) for 5 minutes. The inductance was then measured for different applied positive voltages. The plot of the inductance for different electric fields after poling is shown below in figure 23. At 8kV/cm, the inductance has changed by ~15% at 1 GHz, with a maximum change of 25%, and the FMR frequency has increased. The 4kV/cm plot shows that, although the PMN-PT strain is linear in this regime, [35] the change in inductance is not. The inductance slightly increases (2-4%) with E-field before linearly decreasing with increased field. The most likely reason for this is a misalignment between the easy axis of the magnetic film and the axis of the PMN-PT strain (depicted in figure 24). The initial strain on the magnetic film from the PMN-PT will align the

magnetization of the film along the PMN-PT axis. After they are aligned, the linearly increasing strain will behave as expected, causing a decrease in the permeability by behaving like an effective applied magnetic field along the PMN-PT axis.

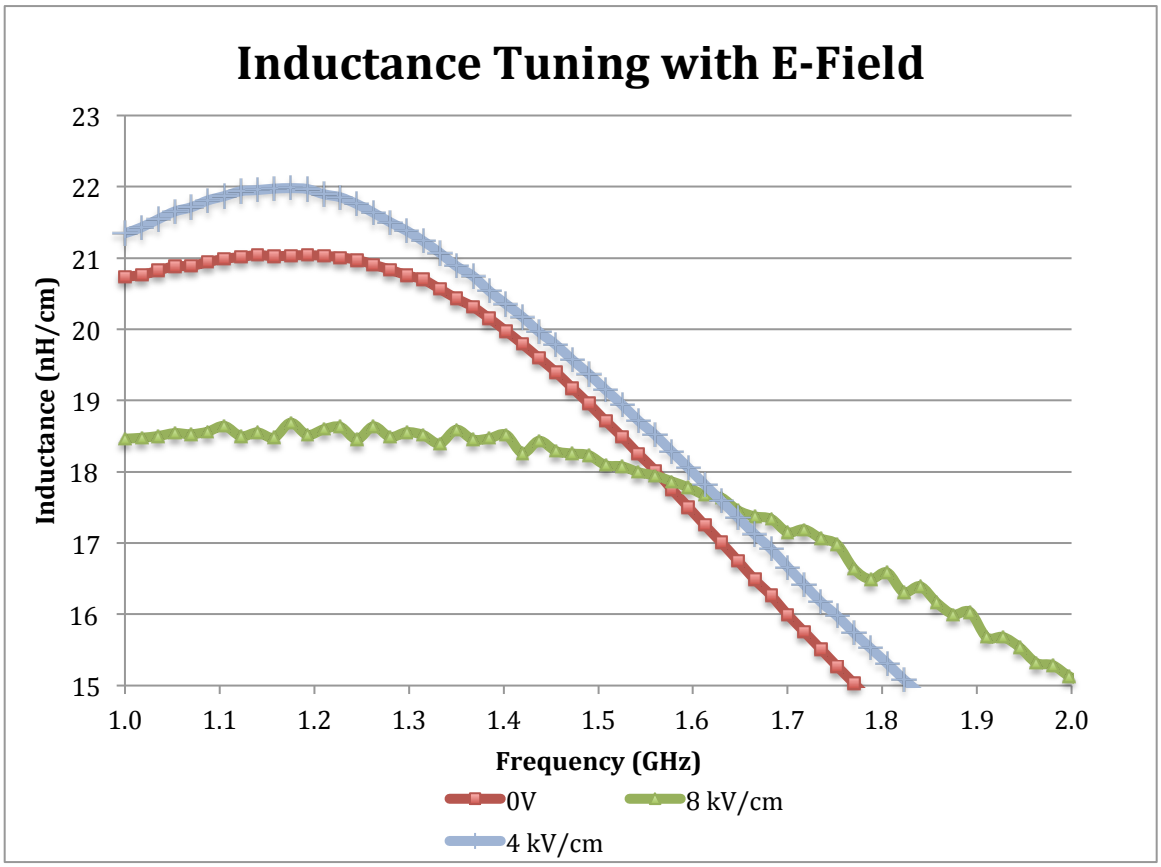

Figure 23: Plot of inductance vs. frequency for the microstrip inductors for different applied voltages demonstrating tuning of the inductance with applied E-field.

Applying an external magnetic field along the easy-axis of the magnetic film and measuring the change in inductance for different applied voltages can confirm this. The results are shown below in figure 25. Not only is the change in inductance significantly smaller because of the applied field, but also a higher voltage is required to enter the linear regime for inductance tuning. Since misalignment results in some of the strain being required to align the magnetization before the inductance can be tuned, there is room for immediate improvements by carefully aligning the layers. If the magnetization

layer is aligned with the PMN-PT strain axes, the inductance should have a linear tuning starting from lower E-fields, resulting in greater tuning range.

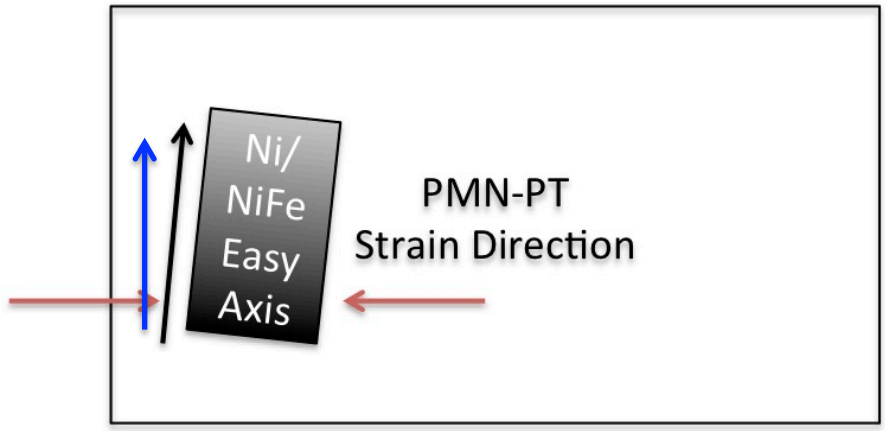

Figure 24: Depiction of the misalignment between the magnetic films and the PMN-PT strain. The strain is depicted with red arrows, the black arrow depicts the easy-axis of the magnetic film, and the blue arrow depicts the effective magnetic field experienced by the devices. Improved tuning will occur when the blue arrow and black arrow are aligned.

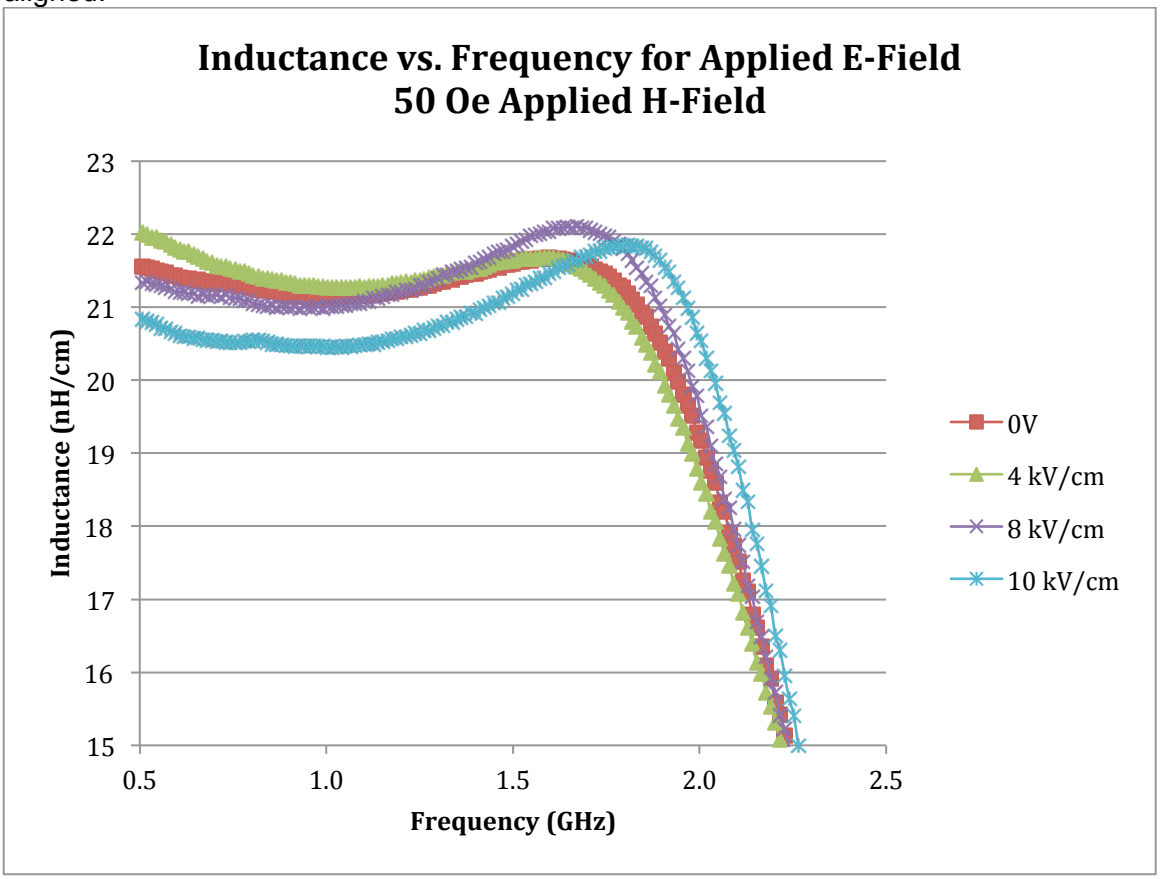

Figure 25: Voltage tuning of the inductors with an applied magnetic field(50 Oe). The magnetic field is applied along the easy axis of the magnetic film. A larger E-field is required to have the linearly decreasing inductance (10 kV/cm)

After the tuning of the inductors was confirmed, they were measured for non-volatile changes. By applying the voltages similar to the strain hysteresis shown in reference 35 (blue curve in figure 15), the inductance can be tuned and then the voltage removed while the inductance change remains. To test this, an electric field of -1.4kV/cm was applied and then removed. Figure 26a shows the first results of this tuning with no applied magnetic field. After the electric field is removed, the inductance stays the same, confirming non-volatile behavior. The inductors can be "erased" by applying a large positive voltage (8kV/cm) and then can be tuned again. This process of writing with -1.4kV/cm and erasing with +8kV/cm was tested and is shown in figure 26b. Once the inductor has been erased, the linear tuning using positive voltages can be used, or the non-volatile tuning using negative fields can be used.

Comparing the magnetic core inductors to the theoretical calculations reveals that the FMR frequency is close to the expected value calculated for the linear combination of the bilayer (1.8 GHz compared to an actual of ~2.4GHz). The tuning range is close (12.4% compared to an actual of 15-25%) and the difference in both values suggest that the estimate for the linear combination of values is low, or the estimated H_a value of 20 Oe is incorrect. The inductance enhancement is less than expected and to improve this new materials need to be used to reduce the magnetic losses affecting the devices. The devices demonstrated GHz operation (enhancement up to ~2.4 GHz with no H-field and E-field), magnetic film enhanced inductance (~75% increase over air-core inductors), tuning of the inductance (15% at 1GHz, with a maximum of 25%) and FMR frequency, enhancement of the quality factor (by ~170%) as well as non-volatile tuning of the inductance.

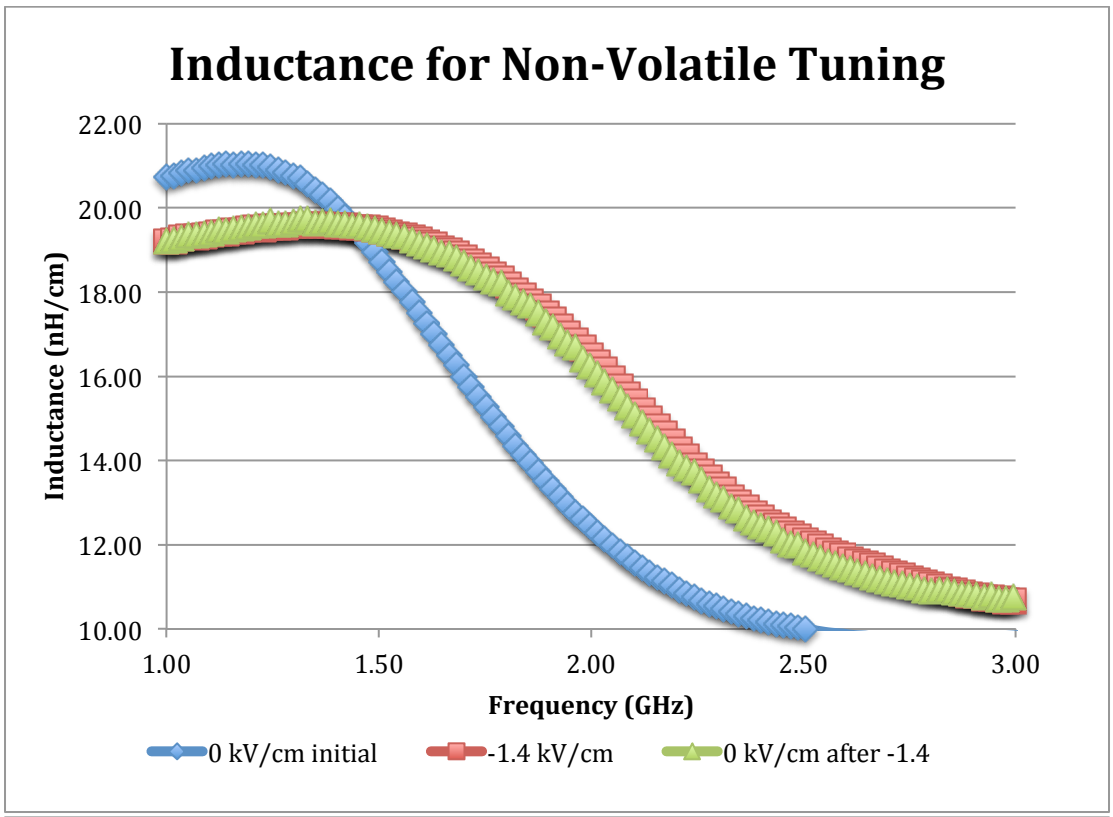

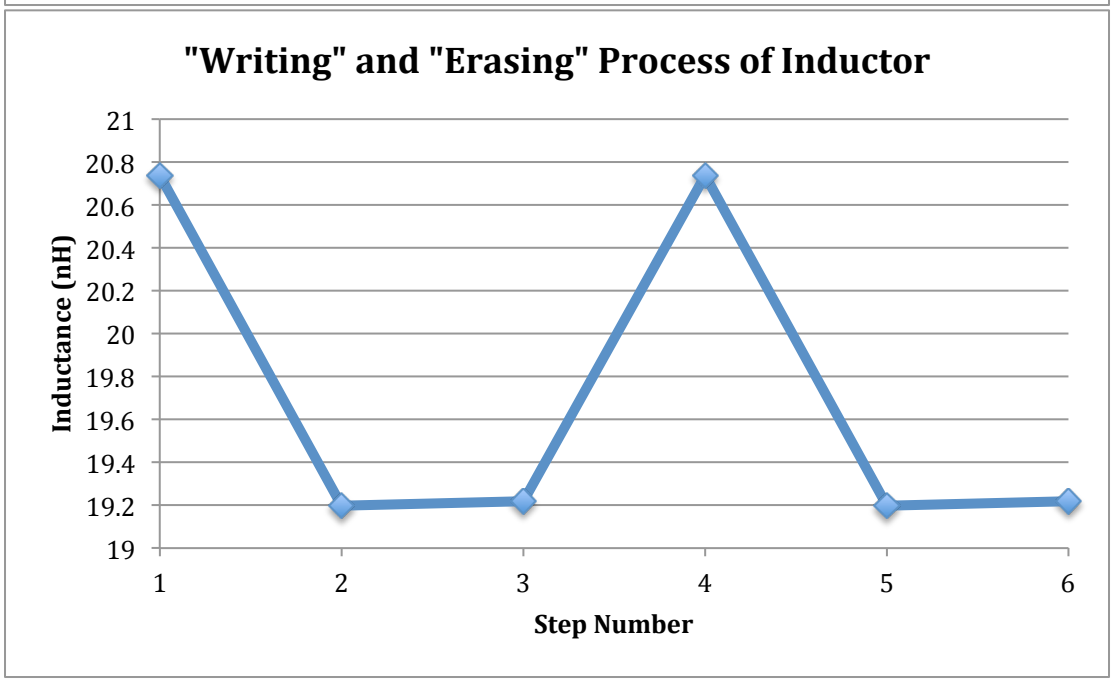

Figure 26: Demonstration of the non-volatile inductance change. (a) Measured inductances demonstrating the non-volatile change at 0V using a -1.4 kV/cm E-field. (b) Repeated "write" and "erase" of the inductance change with voltage steps: (1) 0V initial Inductance, (2) -1.4kV/cm, (3) 0kV/cm tuned inductance, (4) 0V erased inductance after 8 kV/cm applied, (5) -1.4kV/cm, (6) 0 kV/cm tuned inductance

Future Directions

There are many different areas for potential improvement, and depending on the desired application the device properties can be designed and optimized. The frequency was demonstrated in the GHz range (important for many microwave applications), but with a higher resistivity magnetic material as the core, larger inductance gain can be achieved while remaining in GHz operation. Furthermore, the bilayer core (Ni/NiFe) is not the ideal core for both inductance enhancement and for tuning, but rather a compromise for both. By using the bilayer, the magnetic properties are a linear combination of the two materials values [56], reducing Nickel's magnetostriction as well as permalloy's permeability and resistivity. Rather than using one layer with optimal tuning characteristics and one layer with optimal enhancement, a magnetic material can be found that has both high permeability and high magnetostriction (as well as high resistivity and narrow FMR line width). This will allow for significant improvement in both areas, rather than a compromise between the two.

One promising material that can improve the tuning and magnetic enhancement is GaFeB. [19] GaFeB has stronger magnetostriction than Ni(~2x), similar permeability to NiFe, and higher resistivity than both. The higher resistivity would allow for a thicker magnetic core while maintaining GHz operation, and since it has both high permeability and magnetostriction, the magnetic properties would remain high rather than compromise between inductance and tuning. GaFeB also has demonstrated narrow FMR line width, which would improve high frequency operation by reducing losses. [19] When compared with the bilayer core used, a GaFeB core with the same thickness would give >6x's the magnetostriction (increasing tuning range), >2x's the magnetization saturation (improving inductance enhancement), and >3x's the resistivity (reducing high frequency losses). The parameter improvements are summarized in table 5.

Material	Ms	Magnetostriction	Resistivity	FMR frequency	Eddy Loss Frequency
Ni/NiFe	0.9 T	10 ppm	30 μΩ cm	1.8 GHz	3.8 GHz
GaFeB	1.8T	60 ppm	140-180 μΩ cm	2.7 GHz	11 GHz

Table 5: Summary of important magnetic parameters comparing Ni/NiFe Bilayer with GaFeB cores

Conclusion

Magnetic film inductors have shown promise for increasing the inductance density of integrated inductors. Continued improvement of the device characteristics will allow for higher inductances to be used in RF applications, continuing the trend of decreased circuit size and increased electronics portability. The magnetic films need to be easily integrated into CMOS fabrication steps and need improved high frequency performance before they can be used in RF commercial applications.

Research in multiferroics has increased significantly in recent years, particularly in two-phase multiferroics that combine ferroelectricity with ferromagnetism. These two-phase systems show promise for use as sensitive magnetic sensors, energy storage, energy harvesting, magnetic recording devices, and electric and magnetic field tunable microwave devices. Utilizing strain mediated coupling between a ferroelectric and a ferromagnetic, high α_{ME} values have been achieved at room temperature.

The combination of two-phase multiferroics with magnetic film inductors has been investigated for low-energy voltage tuning of inductance. Voltage tuned inductors have been heavily investigated by utilizing MEMS type devices, but little research has gone into multiferroics for tuning. The devices that have been demonstrated utilize an entire multiferroic substrate as the core of a solenoid and have low operating frequencies (<1 MHz). Microstrip inductors were fabricated to demonstrate high frequency operation of voltage tuned magnetic film inductors.

Devices were demonstrated with an inductance enhancement of 75%, tuning range up to 25%, quality factor enhancement of 170%, and operation frequency up to 2.4 GHz. Additionally, by utilizing a strain hysteresis in a PMN-PT (110) substrate, the inductance change can be non-volatile. The "writing" of the inductance using -1.4kV/cm was shown to have a non-volatile change. Furthermore, the "erasing" of the change was demonstrated with the inductance returning to its initial value after an electric field of 8 kV/cm was applied. The inductors are able to have a linear tuning range by utilizing positive voltages, and can have a non-volatile inductance change using the strain hysteresis at -1.4 kV/cm. This gives these inductors a unique ability to have both non-volatile discrete switching (similar to the series inductance tuning previously demonstrated, with the addition of non-volatility) as well as a continuous tuning range at GHz frequencies. The parameters of the fabricated devices are summarized and compared to previously fabricated multiferroic devices in table 6 below.

Initial Inductance	**Tuning Type**	**Tuning Range**	**Quality Factor (0 kV/cm)**	**Actuation Needed**	**Maximum Operating Frequency**
450 µH	Continuous	20%	-	5 kV/cm	10 kHz
1 mH	Continuous	57%	-	3 kV/cm	100 kHz
0.2 mH	Continuous	400%	3	12 kV/cm	1 MHz
21 nH/cm	*Continuous &* ***Non-volatile Discrete***	*25%*	*1.4*	*8 kV/cm*	***2.4 GHz***

Table 6: Comparison of Multiferroic type voltage tuned inductors. The device fabricated for this study is shown as the last entry in italics.

There are many improvements that can be made, from as simple as alignment of magnetic easy axis with the strain axis, to entirely changing the magnetic core material and thickness. The properties of the inductors can be tuned with magnetic materials choice and patterning, as well as the choice for the inductor design. These demonstrated devices show promise for the ability of voltage tuned magnetic film inductors to be used in RF applications with further research.

References

1. Korenivski, V. “GHz Magnetic Film Inductors” *Journal of Magnetism and Magnetic Materials,* 215-216 (2000) 800-806

2. Gardner, Donald S. Gerhard Schrom, Fabrice Paillet, Brice Jamieson, Tanay Karnik, and Shekhar Borkar “Review of On-Chip Inductor Structures with Magnetic Films” *IEEE Transactions on Magnetics*, Vol. 45 (10), 2009

3. Lee, Dok Won. Liangliang Li, Shan X. Wang, Jiongxin Lu, C. P. Wong, Swapan K. Bhattacharya and John Papapolymerou “Embedded Passives” *Materials for Advanced Packaging* (pp. 459-502) New York: Springer Science

4. Jiangtao Sun, Shihai He, Xuewen Zhu, Qing Liu, Toshihiko Yoshimasu. A Novel Variable Inductor Using A Triple Transformer and MOS Switches in 0.13 μm CMOS Technology” *CJMW Proceedings (*2011)

5. B. Assadsangabi, M.S. Mohamed Ali and K. Takahata. “Ferrofluid-based variable inductor” *MEMS 2012*, Paris, FRANCE, 29 January - 2 February (2012)

6. S. Aliouane, A.B. Kouki, R. Aigner “RF-MEMS switchable inductors for tunable bandwidth BAW filters” *2010 International Conference on Design & Technology of Integrated Systems in Nanoscale Era* (2010)

7. N. Saleh, A.H. Qureshi, “Permalloy thin film inductors” *Electron. Lett. 6* (1970)

8. D. S. Gardner, A. M. Crawford, and S. X. Wang, “High frequency (GHz) and low resistance integrated inductors using magnetic mate- rials,” *Proc. IEEE Int. Interconnect Tech. Conf.*, pp. 101–103, (2001)

9. B. Viala, S. Couderc, A. S. Royet, P. Ancey, and G. Bouche, “Bidirectional ferromagnetic spiral inductors using single deposition,” *IEEE Trans. Magn.*, vol. 41, pp. 3544–3549, (2005)

10. A. Gromov, V. Korenivski, D. Haviland, R.B. van Dover, “Analysis of Current Distribution in Magnetic Film Inductors” *Journal of Applied Physics.*, vol. 85, p. 5202 (1999)

11. Dok Won Lee, Kyu-Pyung Hwang, and Shan X. Wang. “Fabrication and Analysis of High-Performance Integrated Solenoid Inductor With Magnetic Core” *IEEE Transactions On Magnetics,* Vol. 44, No. 11 (2008)

12. Y.Shimada, J.Numazawa, Y.Yoneda,A.Hosono: “Absolute Value Measurement of Thin Film Permeability” *J Magn. Soc. Jpn.*, vol. 15, p.327 (1991)

13. J. Lou, D. Reed, M. Liu, and N. X. Sun. “Electrostatically tunable magnetoelectric inductors with large inductance Tunability**”** *Applied Physics Letters* vol. 94, p. 112508 (2009)

14. Chen Yang, Feng Liu, Xin Wang, Jing Zhan, Albert Wang, Tian-Ling Ren, Li-Tian Liu, Haibo Long, Zhengzheng Wu, and Xinxin Li. “Investigation of On-Chip Soft-Ferrite-Integrated Inductors for RF ICs—Part II: Experiments” *IEEE Transactions On Electron Devices*, vol. 56, no. 12 (2009)

15. I. Zaquine, H. Benazizi, J.C. Mage, “Ferrite Thin Films for Microwave Applications” *Journal of Applied Physics*, vol. 64 p. 5822. (1991)

16. Y. Suzuki, R.B. van Dover, E.M. Gyorgy, J.M. Phillips, V. Korenivski, D.J. Werder, C.H. Chen, R.J. Cava, J.J. Krajewski Jr., W.F. Peck, K.B. Do, “Structure and Magnetic Properties of Epitaxial Spinel Ferrite Films” *Applied Physics Letters*, vol. 68 p. 714 (1996)

17. G. Choe and M. Steinback, “Surface Roughness Effects on Magnetoresistive and Magnetic Properties of NiFe Thin Flms“ *Journal of Applied Physics,* vol. 85, no. 8 (1999)

18. Y. Zhuang, M. Vroubel, B. Rejaei, E. Boellaard, J. N. Burghartz, “Investigation of Microstrips with NiFe Magnetic Thin Film (I): Experiment” *Journal of the Magnetics Society of Japan*, vol. 26, no. 12 (2002)

19. Jinsheng Gao, Aria Yang, Yajie Chen, J. P. Kirkland, Jing Lou, Nian X. Sun, Carmine Vittoria, and Vincent G. Harris **“**The effect of boron addition on the atomic structure and microwave magnetic properties of FeGaB thin films” *Journal of Applied Physics*, vol. 105, p. 07A323 (2009)

20. Makoto Munakata, Shin-Ichi Aoqui, and Masaaki Yagi. “B-Concentration Dependence on Anisotropy Field of CoFeB Thin Film for Gigahertz Frequency Use” *IEEE Transactions on Magnetics,* vol. 41, no. 10, (2005)

21. Michael A. Russak, Christopher V. Jahnes, Erik Klokholm, Jo-Won Lee, Mark E. Re, Bucknell C. Webb, “Magnetic and structural characterization of sputtered FeN multilayer films”, *Journal of Magnetism and Magnetic Materials*, Volumes 104–107, Part 3, 2 Pages 1851-1854 (1992)

22. A. Gromov and V. Korenivski. “Gigahertz Sandwich Strip Inductors Based on Fe-N Films: The Effect of Flux Closure at the Flange” *IEEE Transactions on Magnetics*, vol. 46, no. 6, (2010)

23. Y. Zhuang, M. Vroubel, B. Rejaei, J.N. Burghartz “Integrated RF inductors with micro-patterned NiFe core” *Solid-State Electronics* vol. 51 p. 405–413 (2007)

24. Kangho Lee, Jonathan J. Sapan, Seung H. Kang, and Eric E. Fullerton. “Perpendicular magnetization of CoFeB on single-crystal MgO” *Journal of Applied Physics,* vol. 109, p. 123910 (2011)

25. M. Yamanouchi, R. Koizumi, S. Ikeda, H. Sato, K. Mizunuma, K. Miura, H. D. Gan, F. Matsukura, and H. Ohno “Dependence of magnetic anisotropy on MgO thickness and buffer layer in Co20Fe60B20-MgO structure” *Journal of Applied Physics,* vol.109, p. 07C712 (2011)

26. W. Eerenstein, N. D. Mathur, and J. F. Scott, “Multiferroic and magnetoelectric materials” *Nature (London)* vol. 442, p. 759 (2006)

27. R. Ramesh and N. A. Spaldin, “Multiferroics: progress and prospects in thin films” *Nature Materials* vol. 6, p.21 (2007)

28. G Lawes and G Srinivasan. “Introduction to magnetoelectric coupling and multiferroic films” *J. Phys. D: Appl. Phys*., vol. 44 p. 243001 (2011)

29. J. Lou, M. Liu, D. Reed, Y. H. Ren, and N. X. Sun “Electric field modulation of surface anisotropy and magneto-dynamics in multiferroic heterostructures” *Journal of Applied Physics,* vol.109, p. 07D731 (2011)

30. Lee, M. K., Tapan K. Nath, Chang-Beom Eom, Marcia C. Smoak, and Frank Tsui “Strain modification of epitaxial perovskite oxide thin films using structural transitions of ferroelectric $BaTiO_3$ substrate.” *Applied Physics Letters,* vol. 77, p. 3547–3549 (2000)

31. Ming Liu, Shandong Li, Ogheneyunume Obi, Jing Lou, Scott Rand, and Nian X. Sun. “Electric field modulation of magnetoresistance in multiferroic heterostructures for ultralow power electronics” *Applied Physics Letters,* vol. 98, p. 222509 (2011)

32. Kim, S.-K. Jeong-Won Lee, Sung-Chul Shin, Han Wook Song, Chang Ho Lee, Kwangsoo No, “Voltage control of a magnetization easy axis in piezoelectric/ferromagnetic hybrid films.” *J. Magn. Magn. Mater.* Vol. 267, p. 127–132 (2003)

33. Dong, S., Li, J. F. & Viehland, D. “Ultrahigh magnetic field sensitivity in laminates of Terfenol-D and $Pb(Mg_{1/3}Nb_{2/3})O_3$–$PbTiO_3$ crystals.” *Appl. Phys. Lett.,* vol. 83, p. 2265–2267 (2003)

34. Inoue, M. “Magnetophotonic crystals” *Mater. Res. Soc. Symp. Proc.,* vol. 834, p. J1.1.1–J1.1.19 (2005)

35. Tao Wu, Alexandre Bur, Ping Zhao, Kotekar P. Mohanchandra, Kin Wong, Kang L. Wang, Christopher S. Lynch, and Gregory P. Carman. “Giant electric-field-induced reversible and permanent magnetization reorientation on magnetoelectric Ni/„011... †Pb„Mg1/3Nb2/3...O3‡„1−x...–†PbTiO3‡x heterostructure” *Applied Physics Letters,* vol. 98, p. 012504 (2011)

36. Piljae Park, Cheon Sook Kim, Mun Yang Park, Sung Do Kim and Yu. Hyun Kyu, “Variable Inductance Multilayer Inductor With MOSFET Switch Control”, *IEEE Electron Device Letters*, vol. 25, no. 3, p. 144-146. (2004)

37. Zhou, S., X.-Q. Sun and W.N. Carr, “A monolithic variable inductor network using microrelays with combined thermal and electrostatic actuation”, *Journal of Mircomechanics and Microengineering*, vol. 9, no. 1, p. 45-50, (1999)

38. Peroulis, D., S. Pacheno, K. sarabandi and L. Katechi, “Tunable Lumped Components with Applications to Reconfigurable MEMS Filters”, *The*

Proceedings of the IEEE International Microwave Symposium Digest, p. 341-344 (2001)

39. Issam El Gmati, Pierre Francois Calmon, Ali Boukabache, Patrick Pons, Re´my Fulcrand, Ste´phane Pinon, Hatem Boussetta, Mouhamed Adel Kallala and Kamel Besbes. "Fabrication and evaluation of an on-chip liquid micro-variable inductor" *Journal Micromechanics and Microengineering*, vol. 21, p. 025018, (2011)

40. Mina Rais-zadeh, A. Kohl, Farrokh Ayazi, "MEMS Switched Tunable Inductors", *IEEE Journal of microelectromechanical systems,* vol. 17, no.1, p. 78-84 (2008)

41. Owen Casha, Dominique Morche, "Utilization of MEMS Tunable Inductors in the Design of RF Voltage-Controlled Oscillators", *The Proceedings of the 15th IEEE International conference on Electronics, circuits and systems*, p. 718-721 (2008)

42. Ning, N., X.P. Li, J. Fan, W.C. Ng, Y.P. Xu, X. Qian and L. Seet, "A Tunable Magnetic Inductor", *IEEE Transactions on Magnetics*, vol. 42, no. 5, p. 1585-1590 (2006)

43. Sarkar, N., D. Yan, M. Ellias, E. Horne, J.B. Lee, H. Lu, R. Mansour, A. Nallani, G. Skidmore, "Microassembled Tunable MEMS Inductor" *The Proceedings of the 18th IEEE International conference on Microelectromechanical Systems*, p. 183-186, (2005)

44. Teymoori, M.M., J. Merrikhi Ahangarkolaei, "Design and Simulation of a novel electrostatic MEMS tunable inductor for RF applications", *The Proceedings of the 3rd international conference on computer engineering*, p. 825-831 (2011)

45. Jeong-Il Kim. and Dimitrios Peroulis, "Tunable MEMS Spiral Inductors with Optimized RF Performance and Integrated Large-Displacement Electrothermal Actuators", *IEEE Transactions On Microwave Theory and Techniques*, vol. 15, no. 9, p. 2276-2283 (2009)

46. Imed Zein-El-Abidine, Michal Okoniewski and John G. McRoy, "RF MEMS Tunable Inductor Using Bimorph Microactators", *The Proceedings of the IEEE International conference on MEMS, NANO and Smart Systems*, p. 1-2 (2005)

47. Imed Zein-El-Abidine, Michal Okoniewski and John G. McRoy, "A New Class of Tunable RF MEMS Inductors", *The Proceedings of the IEEE International conference on MEMS, NANO and Smart Systems*, (2003)

48. Usama Zaghloul, Amal Zaki, Hamed Elsimary, Hani Ghali, and Hani Fikri, "Design of MEMS Tunable Inductor Implemented on SOI and Glass Wafers Using Bonding Technology", *The Proceedings of the WSEAS International conference on Microelectronics, Nanoelectronics and Optoelectronics*, p. 157-163 (2006)

49. Yutaka Mizuochi, Shuhei Amakawa, Noboru Ishihara and Kazuya Masu, "Study of air-suspended RF MEMS Inductor Configurations for Realizing Large Inductance Variations", *The Proceedings of the IEEE Argentine School of Micro-Nanoelectronics, Technology and Applications conference*, p. 50-55 (2009)

50. Issam Gmati, Hatem Boussetta, Mohamed Adel KAllala and Kamel Besbes, "Wide-range RF MEMS Variable Inductor Using Micro Pump Actuator", *The Proceedings of the 2nd International conference on signals, circuits and systems*, p. 1-4, (2008)

51. Dong-Hoon Choi, Hyung Suk Lee and Jun-Bo Yoon, "Linearly Variable Inductor with RF MEMS Switches to Enlarge A Continuous Tuning Range", *The Proceedings of the 15th International conference on soild-state sensors, actuators and Microsystems*, p. 573-576, (2009)

52. X. Fang, N. Zhang, and Z. L. Wang. "Converse magnetoelectric effects on heterotype electrostrain-piezopermeability composites" *Applied Physics Letters* vol. 93, p. 102503 (2008)

53. Guoxi Liu, Xiaoxi Cui, and Shuxiang Dong. "A tunable ring-type magnetoelectric inductor" *Journal of Applied Physics,* vol. 108, p. 094106, (2010)

54. Na An, Albrecht Jander, and Pallavi Dhagat. "Electrically Tunable Thin Film Magnetic Core Using Synthetic Antiferromagnet Structure" *IEEE Transactions on Magnetics*, vol. 44, no. 11, (2008)

55. Pedram Khalili Amiri, Behzad Rejaei, Yan Zhuang, Marina Vroubel, Dok Won Lee, Shan X. Wang, and Joachim N. Burghartz. "Integrated Microstrip Lines With Co–Ta–Zr Magnetic Films" *IEEE Transactions on Magnetics*, vol. 44, no. 11, (2008)

56. A. Gerber, J. McCord, C. Schmutz, and E. Quandt. "Permeability and Magnetic Properties of Ferromagnetic NiFe/FeCoBSi Bilayers for High-Frequency Applications" *IEEE Transactions on Magnetics*, vol. 43, no. 6, (2007)

57. P Poulopoulos and K Baberschke "Magnetism in Thin Films." *J. Phys.: Condens. Matter*, vol. 11, p. 9495–9515, (1999)

58. Charles R. Sullivan, Satish Prabhakaran, Parul Dhagat, Yuqin Sun "Thin-Film Inductor Designs and Materials for High-Current Low-Voltage Power" *2nd International Symposium on High-Frequency Micromagnetic Devices and Materials*, (2003)

59. I. Iramnaaza, T. Sandovala, Y. Zhuanga, H. Schellevisb, B. Rejaei, "High Quality Factor RF Inductors Using Low Loss Conductor Featured with Skin Effect Suppression for Standard CMOS/BiCMOS" *Electronic Components and Technology Conference*, (2011)

60. Amikam Aharoni, "Demagnetizing factors for rectangular ferromagnetic prisms" *Journal of Applied Physics,* vol. 83, no. 6, (1998)

61. Marina Vroubel, Yan Zhuang, Behzad Rejaei, Joachim N. Burghartz, Ankur M. Crawford, and Shan X. Wang, "Calculation of Shape Anisotropy for MicropatternedThin Fe–Ni Films for On-Chip RF Applications" *IEEE Transactions on Magnetics*, vol. 40, no. 4, (2004)